Technische Universität Braunschweig

Institut für Festkörpermechanik

Master Thesis

An inverse finite element approach to characterize the mechanical properties of hydrogels

May 13, 2013

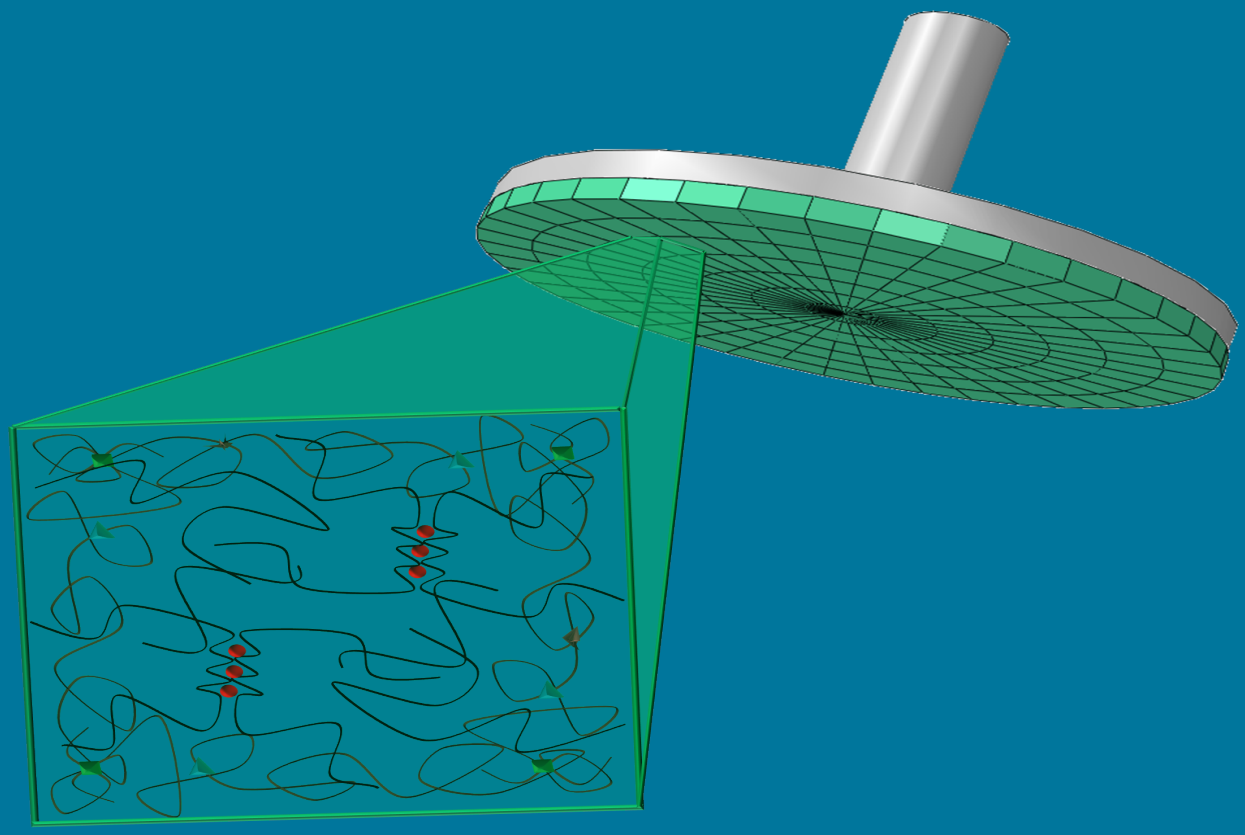

Xabier Ocáriz Aguirre

Contents

List of Figures

List of Tables

1 Introduction

Biofilms grow on various surfaces and in many different enviroments, a phenomenon that leads to major problems in fields of industry and medicine. The mechanical stability of biofilms and other microbial aggregates is of great importance for both the maintenance of biofilm processes and the removal of undesired biofilms. Biofilms are defined as communities of microorganisms that exist in close association with interfaces and are embedded in a matrix of self-produced extracellular polymeric subtances(EPS)[8]. They can be benign and be involved in self-cleaning processes of wastewater and soil or for productive and stable fermentation processes. On the other hand they can be pathogenic by its role in the development and persistence of infectious diseases, such as colonizing the respiratory tract or implanting devices.

Biofilm's architecture is provided by this extracellular polymeric substances(EPS). EPS are a mix of polysaccharides, proteins, lipids and nucleic acids[9]. They are considered to be the components that determine the structural and functional integrity of microbial aggregates. The forces responsible for the adhesion of biofilms on surfaces and the stability of the biofilms matrix are caused by hydrogen bonds, dispersion forces and electrostatic interactions[10]. For this reason, it is necessary to know the mechanical properties of biofilms in order to be able to control biofilms formation. Mechanical properties influence how biofilms respond to external forces, cell detachment and dispersal from biofilms and mass tranfers into biofilms.

The aim of this Thesis is to achieve and to obtain, a rheological characterization of hydrogels by means of the finite element method, the parameters which define the biofilm model that has been implemented in ABAQUS software by Ehret[5]. The idea of characterizing hydrogels comes from the the rheological test that have been carried out in the biotechnology institute(ibvt), specifically in the Master Thesis of Daria Kaptsan[11]. His work is focused in establishing the hydrogel as a biofilm model. Biofilms have the EPS matrix character as gel and show similar reversible deformation as hydrogels. The effect of divalent cations such as Mg and Ca was checked on the gel strength. Finally they immobilized *Pseudomonas Putida KT2440* cells inside the gel to simulate the biofilm behaviour under mechanical stress.

Therefore it is in ABAQUS software where the frequency sweep that tests the rheometer used in the laboratories of biotechnology to get the parameters which define the mechanical behaviour of hydrogels is simulated and compared against experimental data. It started out from an overview of past research on biofilm mechanics listed in section 2.3 to focus on the rheological tests and specifically in oscillation tests.

In chapter 3 the main mathematical models that represent the viscoelastic behaviour are introduced. These are the basis to create models as the one implemented for the finite element software. Together with this, it explains the principles of continuum mechanics at large strains. With these knowledge the mechanical model of biofilm developed by Ehret can be presented. This model is the basis of the subroutine which is then implemented in ABAQUS to carry out the simulations.

In order to understand and be able to model the frequency sweep it is briefly described in chapter 4 the rheologic basis. The theory is focused on the oscillation tests from rotational rheometers. Every type of geometry used in these tests is listed. In particular, the CS-Bohlin rheometer, which has been used in tests that are modeled, is described. The "form factors" used for converting the "instruments numbers" to "rheological numbers" are shown for the plate-plate geometry in section 4.4.

Within chapter 5 it is justified the design of the two models which are simulated in ABAQUS. These are the models that represent a uniaxial compression test and a frequency sweep. The simulated compression test is based on the paper of Ehret[5] and the frequency sweep in the research of Kaptsan[11].

With the designed simulations, the first thing that is done is the check of the response provided by the FEM subroutine through a compression test. The same compression test is simulated with the parameters of a *Pseudomonas aeruginosa* biofilm and compared against the graphs ilustrated on that paper. Then the simulated frequecy sweep is validated again at the light of the analytical results obtained from *Pseudomonas aeruginosa* biofilm. Both results are discussed in section 6.1 and section 6.2.

Finally with the frequency sweep model validated, in section 6.3, the biofilm model parameters that define the behaviour of hydrogel with the influece of divalent cations such as Mg and Ca are obtained. To this end, the simulations are based on certain assumptions of mechanical researches on Gellan, which is the gel used in the rheological tests. The influence by varying certain parameters that define the material, as are the number of chains per network or the relaxation times of these chains, is studied in order to reach an estimation of these parameters. Lastly, in conclusion, it is compared the curves obtained by these simulations on finite elements against the ones obtained by the rheometer by Kaptsan[11].

2 Biological Background

2.1 Biofilms

Biofilms are an aggregate community of microorganisms and extracellular polymeric substances(hereinafter EPS) fixed to a surface, as it is showed in figure 2.1 where it is clearly appreciated either a single species or a range of different ones[12]. They just need an hydrated environment and a minimal presence of nutrients because they can grow on hydrophobic or hydrophilic, biotic and abiotic surfaces.

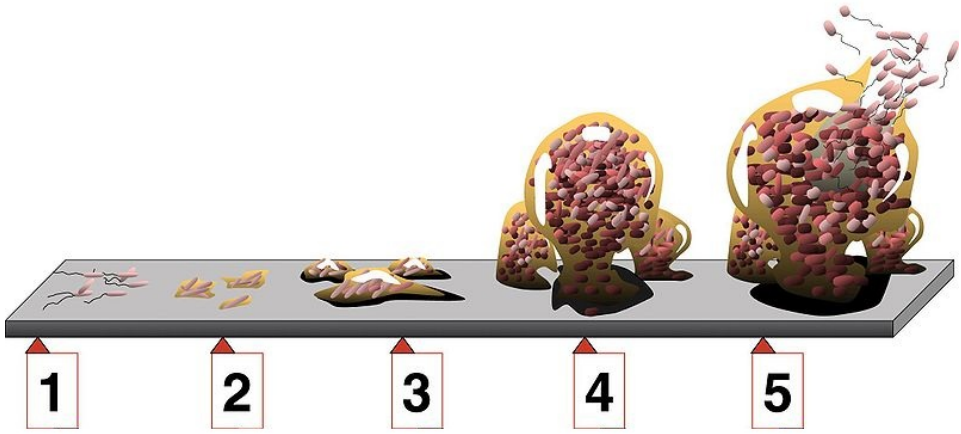

Figure 2.1: Development of biofilm, in this case for *Pseudomonas Aeruginosa*, shows five stages: 1. Initial attachment; 2. Irreversible attachment; 3. Maturation I; 4. Maturation II; 5. Dispersion. (Monroe,2007)[1]

Biofilms incorporate large amounts of water within its structure. This element comes to represent up to 97% of the biofilm. Besides water and germs, the matrix consists of exopolysaccharides, which constitute its essential component, produced by the microorganism's members themselves. Regardless, there are other macromolecules in a smaller amount, such as proteins, nucleic acids and diverse products derived from bacterial matter. The matrix materials may also be bacterial, such as crystals of inorganic salts, corrosion particles or sediment and blood components, as well as the environment in which biofilm growths. Bacterial cells are compress about 15% - 20% of the volume and cannot be divided into biofilms.

The set of polysaccharides, nucleic acids and proteins are known as the extracellular

polymeric substances(EPS). The mechanical stability of biofilms is highly dependent on the EPS[10]. The forces which are responsible of the adherence of the biofilm to the surface and the stability of the matrix, are based on hydrogen bonds, electrostatic interactions, and dispersion forces. Furthermore, the EPS may be associated with metal ions and divalent cations[13].

We could find biofilms in all habitats where bacteria exist: in the environmental, clinical or industrial fields among others. Their mere existence can be either harmful to us (equipment fouling, generation of harmful metabolites) or beneficial for our purposes (wastewater treatment, biochemical production).

On the one hand, in medically-related fields, biofilms play an important role in the development and persistence of infectious diseases[14] . More than 60% of the bacterial infections currently treated by physicians in developed countries occur due to biofilm formation. Oral biofilms are known to cause dental caries and periodontitis. Aquatic bacteria *Pseudomonas aeruginosa* can colonize lower respiratory tract and instigate cystic fibrosis pneumonia. Biomaterial-related infections occur when microorganisms inhabit medical devices, such as catheters, prostheses and heart valves.

On the other hand we can take advantage of biofilms in other areas. Some water treatment plants(waste and food industries) act by imitation of the naturally occurring processes in the environment, in which a biofilm is responsible for maintaining and recovering the water quality. Moreover it also biodegrades the organic material and most of the toxic compounds and thus act as detoxifying agents. They are also useful for monitoring these compounds in the environment in which they live[15]. Another case is the immobilization of microorganisms for the production of industrial products. The biofilm is the natural habitat of microbes; its shows an innate tendency to mucous membranes immobilized in these structures and organizes them in complex communities able to produce certain substances in excess. This ability has been the basis of industrial bioreactors[16], which are closed systems that use microorganisms for productive and stable fermentation processes.

2.2 Pseudomonas Putida KT2440

Pseudomonas Putida is a metabolically versatile saprophytic soil bacterium that has been certified as a biosafety host for the cloning of foreign genes. The bacterium also has considerable potential for biotechnological applications. It demonstrates a very diverse metabolism, including the ability to degrade organic solvents such as toluene[17]. This ability has been applied in bioremediation, or in the the use of microorganisms to biodegrade oil.

The strain *Pseudomonas Putida KT2440* is a mutant deficient DNA restriction system of

the strain *P. putida mt-2* originally isolated in Japan. This one carries the plasmid TOL: pWW0, which encodes a degradation pathway of toluene and xylene which is one of the best characterized in the field of the biodegradation basis of biochemical and genetic aspects. Sequence analysis of the 6.18 Mb genome of strain KT2440 reveals diverse transport and metabolic systems. The analysis of the genome gives us an insight into the non-pathogenic nature of *P. putida* and gives us a hint of potentially new applications in agriculture, biocatalysis, bioremediation and bioplastic production[18].

An important aspect of the research on genus of the *Pseudomonas putida KT2440* is that there is a high level of genome conservation with the pathogenic *Pseudomonas aeruginosa*(85% of the predicted coding regions are shared), key virulence factors including exotoxin A and type III secretion systems are absent.

2.3 Biofilm Testing Techniques

Mechanical properties influence how biofilms respond to external forces, cell detachment and dispersal from biofilms and mass transfer into biofilms. In order to be able to model biofilm behavior and, potentially, be able to control biofilms formation, it is necessary to know the mechanical properties of biofilms.

Measurements of biofilms mechanical properties and the interpretation of the results are complicated due to the structural and biological heterogeneity of biofilms, usually containing multiple species of microorganisms and complex networks of channels and voids. Currently, no standard method for measuring the mechanical properties of any kind of biofilms have been developed so far. However, in an attempt to quantify biofilms mechanical properties, various methods have been used[19]. An overview of past research on biofilm mechanics is summarized below.

The first reported study of biofilm mechanical properties was performed by Characklis[20]. He conducted rheological measurements with Weissenberg rheogoniometer in situ, on mixed biofilm population. Weissenberg rheogoniometer is a cone and plate rheometer capable of measuring both viscous and elastic responses of polymers. The tangential force caused by resistance to flow when the cone turns with respect to the plate is a measure of the viscous flow. The normal force perpendicular to the plane of rotation represents elasticity. Biofilms were grown on the plates, placed in the instrument and subjected to oscillating shear. Characklis[21] reported that biofilms exhibited viscoelastic behavior similar to the behavior of a cross-linked protein gel with the same water content as the biofilms.

The work of Characklis was followed by Ohashi and Harada[22], who studied tensile and shear adhesion strength of denitrifying biofilms. Tensile force was created by centrifugation of biofilm attached plates, while shear force was generated by colliding biofilm

attached plates by gravity. They reported that both biofilm tensile and shear adhesion strengths declined with biofilm age. The weakest place of the biofilms was found at the substratum interface. Their study threw some light over the difference in terms of magnitude between shear and tensile strength, stating that this last one was two orders lower than the first one. Ohashi[23] developed a tensile test device for measuring tensile strength of denitrifying biofilms. They concluded that biofilm tensile strength was independent of biofilm density and EPS content. They also found a strong correlation between biofilms elastic coefficients and their tensile strength, suggesting that biofilms can be considered as an elastic material. Stoodley[24] conducted stress-strain and creep experiments on mixed and pure culture biofilms using controlled fluid shear in combination with digital time lapse microscopy. These experiments came to confirm Characklis's theory which declared that biofilms possessed viscoelastic properties and discovered that biofilms behaved like elastic and viscoelastic solids below the shear rate at which they were grown but in counterpoint behaved like viscoelastic fluids at higher shear rates. In another study, Klapper and co-workers[25] demonstrated again that biofilms are viscoelastic fluids with irreversible flow at long deformation times with elastic and viscoelastic recovery, which can be modeled as Jeffrey's viscoelastic fluids. Biofilm shear strength was studied using cone and plate rheometer by Towler and colleagues[26], who showed that biofilms had a behavior which is common to viscoelastic fluids so they used a 4-linear viscoelastic Burger element to model it.

In addition to shear and tensile testing, compression testing was used in biofilm mechanics. Korstgens and co-workers[27] used an uniaxial compression measurement device to study mechanical behavior of *P. aeruginosa* biofilms. They measured biofilms until their failure point and derived biofilm's apparent modulus of elasticity and yield strength from their experiments. They also confirmed that biofilms were viscoelastic materials and showed that yield strength and modulus of elasticity are influenced by the addition of calcium ions.

Strength of adhesion between biofilms and surfaces was measured by Chen and co-workers[28]. They used a micromanipulator on the biofilms of *P. fluorescens* and found that adhesive strength was affected by growth conditions, i.e. pH, nutrient concentration, surface roughness, age, and, the most important, fluid shear at growth. Biofilms grow stronger adhered to the surface at higher shear.

The cohesive strength of biofilms was measured by Poppele and Hozalski[29] with the micro-cantilever method, by Ahimou and colleagues[30] with atomic force microscopy (AFM) and by Mohle and colleagues[31] with fluid dynamic gauging. Poppele and Hozalski obtained a range of values for cohesive strength of activated sludge, which in quantity were much higher than those measured by Ahimou and colleagues. Ahimou et al. showed that calcium ions influenced cohesive strength of biofilms. Mohle et al. used activated sludge biofilms for their tests and reported values that happened to be in an intermediate stage between those obtanied by Poppele and Hozalski and the ones reached by Ahimou et al., which were 200 to 1,100 higher than shear forces at biofilm growth.

Several attempts were made to model biofilm mechanical behavior. Picioreanu and colleagues[32] used a two-dimensional model for biofilm growth and as a result they evaluated the effect of detachment on biofilm structures. Their model generated a variety of realistic biofilm-formation patterns. They showed that erosion(small-particle loss) made the biofilm surface smoother, and sloughing(large biomass-particle removal) increased surface roughness. Their results showed that biofilm sloughing was affected by its strength and shape, and suggested that sloughing could be minimized by the application of high liquid shear, always verifying that biomass growth rates were low.

In conclusion, biofilms studies showed that biofilm strength was affected by increasing EPS production[9], EPS chemistry[7] and the presence of divalent cations[33], growth medium, hydrodynamic conditions during growth[8] and quorum sensing[34]. However, the majority of the studies were conducted with environmental biofilms. Mechanics of medically-relevant biofilms received less attention, despite their great importance concerning human quality of life.

3 Mechanical Background

When biofilms are subjected to forces, they behave elastically over short periods of time(seconds) and there is a nonlinear relationship between applied force and resulting strain, while deformations are reversible. Viscoelasticity is the property of materials that exhibit both viscous and elastic behavior when undergoing deformation. At high deformations, biofilms show viscoelastic behavior by resisting applied forces and displaying irreversible deformation[7].

For this reason, in this chapter it is summarized the fundamentals of viscoelasticity and presented the main viscoelastic models. It is also introduced basis for understanding the large strain continuum mechanic, a type of nonlinear elasticity. Finally, and from these bases, it is described the mechanical model which is implemented in the subroutine that represents the mechanical behavior of microbial biofilm.

3.1 Viscoelastic Model

The classical theory of elasticity considers the mechanical properties of the elastic solids according to Hooke's law. This means that the deformation is achieved directly proportional to the applied stress. Moreover, the hydrodynamic theory discusses about properties for viscous liquids which, according to Newton's law, the force applied is directly proportional to the strain rate, and independently of the own deformation.

These two categories are idealizations; generally the behaviour of many solid approximates by Hooke's law(elastic behaviour) in infinitesimal deformations and many liquids approximates by Newton's law(viscoelastic behaviour) for low strain rates. As a result, if a stress is applied on an elastic solid, it deforms until the deformation force ceases and returns to its initial value. On the other hand, if a stress is applied to a viscous fluid, it is deformed, but recovers nothing that its shape. An intermediate behaviour is viscoelastic behaviour, wherein the body on which is applied effort recovers part of the applied strain. These three behaviors are shown in figure 3.1

The development of the mathematical theory of linear viscoelasticity relies on the principle in which the response(strain) at any time is directly proportional to the driving force(stress). Thus, if the deformation and strain rate are infinitesimal, and the relation between stress-strain are time-dependent, we have linear viscoelastic behaviour.

The relation between stress and deformation considering its dependence time is given

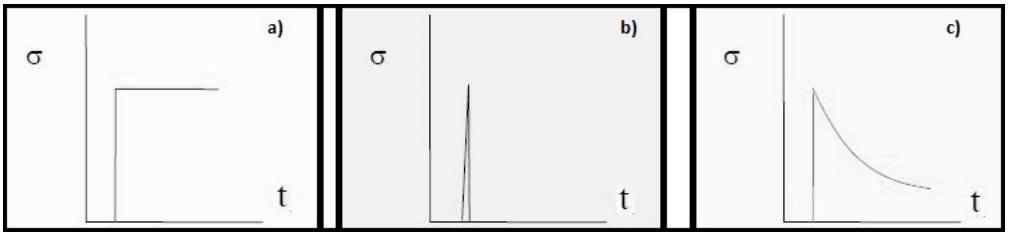

Figure 3.1: Stress-Time graphs for: a) Solid approximates by Hooke's law ; b) Liquid approximates by Newton's law; c) Viscoelastic time-depedent material. Each one of the graphs represent the response of the stress σ, over time t, applying an instantaneous deformation according to the material model used. (Moreno, 2000)[2]

by the state equation. For a system subjected to a simple shear, the equation constituent can be written as[35]:

$$\tau(t) = \int_{-\infty}^{t} G(t - t^{'}) \frac{\mathrm{d}\gamma(t^{'})}{\mathrm{d}t^{'}} \mathrm{d}t^{'} \tag{3.1}$$

where t is the current time and $t^{'}$ is a moment before any process; $G(t)$ is defined as the relaxation modulus. An alternative form of this equation is written using the function memory $M(t - t^{'})$:

$$\tau(t) = \int_{-\infty}^{t} M(t - t^{'}) \gamma(t, t^{'}) \mathrm{d}t^{'} \tag{3.2}$$

As noted in each one of the above expressions, the integrands consists of two terms: one characteristic of the material and another characteristic of the deformation process. It should be noted that both $M(s)$ and $G(s)$, where $s = t - t'$, are functions that tend to zero as s goes to infinity.

The linear viscoelastic theory is based on **the Boltzmann superposition principle** by which the response(e.g. strain) at a given time is proportional to the initial signal value(e.g. stress), i.e. doubling the deformation, effort is doubled. The differential equations that describe linear viscoelasticity are linear and their coefficients are constant. These constants represent material properties such as viscosity or the elastic modulus, and remain constant when changing variables, such as deformation or strain rate. As a result of these restrictions the linear theory can be applied only when changes in the variables are very small.

This way we can define a general equation describing the linear viscoelasticity as follows in which τ represents the shear stress; γ the shear strain and α_n and β_n represent the ma-

terial constant coefficients[3]:

$$\left(1+\alpha_1\frac{\partial}{\partial t}+\alpha_2\frac{\partial_2}{\partial t^2}+...+\alpha_n\frac{\partial^n}{\partial t^n}\right)\tau=\left(\beta+\beta_1\frac{\partial}{\partial t}+\beta_2\frac{\partial_2}{\partial t^2}+...+\beta_n\frac{\partial^m}{\partial t^m}\right)\gamma \quad (3.3)$$

where $n=m$ or $n=m-1$, the equation simplifies to:

$$\tau=\beta_0\gamma+\beta_1\frac{d\gamma}{dt} \quad (3.4)$$

With this simplification of the equatio 3.3 is possible make use of analogies with simple mechanical models consisting of springs represented by β_0 (elastic behavior) and dashpot represented by β_1 (viscous behavior). These analogies make it possible to have some conceptual insight into the physical behavior of complex materials by breaking down the dissipative viscous processes (time-dependent) and energy-storage processes.

When $\beta_1=0$ in equation 3.4, we obtain the elasticity equation in Hooke's solid where $\beta_0=G$ is represented by a spring(elastic behavior) and G is the value for the shear modullus.

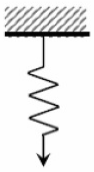

Figure 3.2: Graphic representation for a Hooke's solid with one spring. (Schramm,2004)[3]

If β_1 is the non-zero parameter in equation 3.4, we have the equation for a Newtonian fluid where $\beta_1=\eta$ is represented by a dashpot(viscous behavior) and η is the value for viscosity.

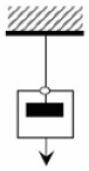

Figure 3.3: Graphic representation for a Newtonian fluid with one dashpot. (Schramm,2004)[3]

It may happen that both variables in equation 3.4, β_0 and β_1, are different from zero, in which case, the equation takes the form:

$$\tau = G\gamma + \eta\dot{\gamma} \tag{3.5}$$

where $\dot{\gamma}$ is the shear strain and represents $\frac{d\gamma}{dt}$.

This is **the Kelvin-Voigt's model** which is one of the simplest in viscoelasticity and is obtained as parallel combination of a spring and a dashpot. If instantaneous stress (τ_0), is applied at $t = 0$ and kept constant, the model satisfies the Kelvin equation

$$\gamma(t) = \frac{\tau_0}{G}\left[1 - \exp\left(-t/\lambda_{\mathrm{k}}\right)\right] \tag{3.6}$$

where λ_k is the Kelvin's delay time. This time constant means that while in the solid Hooke the end value is reached instantaneously, in the deformation of a Kelvin model there is delay until the final value is reached.

In Kelvin model the spring extension is equal to the extension of the dashpot, it means, deformation of the elastic element (spring), represented by γ_e, and deformation of the viscous element (dashpot), represented by γ_v, are equal each other and equal to the total deformation. Furthermore, in the model of Kelvin, the total stress is equal to the sum of the stresses of both elements, where τ_e represents the elastic stress and τ_v represents the viscous stress.

$$\gamma = \gamma_{\mathrm{e}} = \gamma_{\mathrm{v}} \tag{3.7}$$

$$\tau = \tau_{\mathrm{e}} + \tau_{\mathrm{v}} \tag{3.8}$$

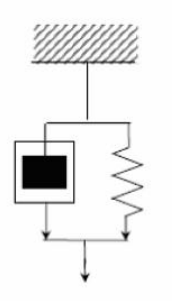

Figure 3.4: Graphic representation for Kelvin-Voigt's model. This model is generated by one spring and one dashpot both in parallel. (Schramm,2004)[3]

Another model of viscoelasticity is called **the Maxwell's model**, in which the non-zero parameters in equation 3.3 of the material are $\alpha_1 = \lambda$ and $\beta_1 = \eta$, whereby the resulting

differential equation is

$$\tau + \lambda_M t = \eta\dot{\gamma} \tag{3.9}$$

where λ_M is the rate constant called Maxwell's relaxation time.

Applying an instantaneous strain rate (γ_0), at time $t = 0$ and maintained over the time, the stress is given by

$$\tau = \eta\gamma_0 \left[1 - \exp\left(-t/\lambda_M\right)\right] \tag{3.10}$$

This implies that the deformation stress applied is delayed in its growth. If the strain rate has had a constant value (for $t < 0$) and suddenly ($t = 0$) is eliminated, it results

$$\tau = \eta\gamma_0 \exp\left(-t/\lambda_M\right) \tag{3.11}$$

and then the stress relaxes exponentially to its equilibrium value zero.

The Maxwell's model can be described by a series combination of a spring and a dashpot. In this case, the deformation (or strain rate) are additive, while the total stress is equal to the stress of each element.

$$\gamma = \gamma_e + \gamma_v \tag{3.12}$$
$$\tau = \tau_e = \tau_v \tag{3.13}$$

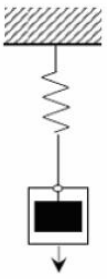

Figure 3.5: Graphic representation for Maxwell's model. This model is generated by one spring and one dashpot both in series. (Schramm,2004)[3]

The next model according in complexity is called **the Burger's model**, in which there are four simple elements whose constitutive equation, derived by equation 3.3 has the form

$$\tau + (\lambda_1 + \lambda_2)\dot{\tau} = \lambda_1\lambda_2\ddot{\tau} = (\eta_1 + \eta_2)\dot{\gamma} + (\lambda_2\eta_1 + \lambda_1\eta_2)\ddot{\gamma} \tag{3.14}$$

This is a second order differential equation where it is related the derivates of first $(\dot{\tau}, \dot{\gamma})$ and second order $(\ddot{\tau}, \ddot{\gamma})$ of both the shear stress (τ) and shear strain (γ). The time constants are represented by λ_1 and λ_2. Also the viscosity of both dashpot are represented by η_1 and η_2.

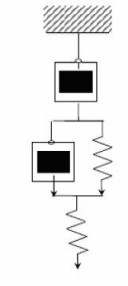

Figure 3.6: Graphic representation for Burger's model. This model is generated by one spring and one dashpot both in parallel and joined with one spring and one dashpot in series. (Schramm,2004)[3]

The Burger's model is represented by two pairs spring/dashpot, one in series and one in parallel. This model describes all the basic features of interest in a viscoelastic fluid. Although more complex models can be established by combining multiple elements of Kelvin-Voigt and Maxwell. In general, Kelvin-Voigt's models are combined in series and Maxwell's models are combined in parallel.

3.2 Large Strain Continuum Mechanics

It is studied the strain of a deformable continous body as we consider the biofilm sample as a deformable body. This body is under action of external loads causing large deformation, so it is no acceptable that the deformed position coincides with the starting position.

Therefore the body is highly nonlinear because the presence of large strains that involves the use of appropiate deformation measurements which are essentially nonlinear. It is necessary to follow an incremental load process, applying loads step by step and determining the response to each of these increments. In order to identify the differents steps of the process it will be used a time parameter t, which will refer all of the load increments and different deformed configuration.

The following figure shows the solid referred to a cartesian coordinate system, and in it are identified:

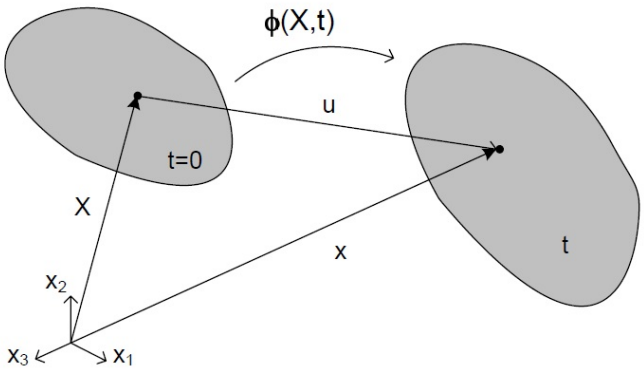

Figure 3.7: Representation of initial and deformed configuration of a solid in cartesian coordinate. The function $\phi(\mathbf{X}, t)$ defines a coordinate transformation between the two spatial configurations. (Celigueta,2008)[4]

Displacement between $t = 0$ and t can be represented mathematically as function:

$$x = \phi(\mathbf{X}, t) \tag{3.15}$$

For each step time, the function ϕ defines a coordinate transformation between the two spatial configurations, start and end. For any particle, the above equation gives the temporal trajectory.

In the Lagrangian configuration it is expressed the final coordinates of a particle as a function of its initial coordinates. The deformation of the body also can be expressed as a function of these coordinates:

$$u(\mathbf{X}, t) = \phi(\mathbf{X}, t) - \mathbf{X} \tag{3.16}$$

This approach pursued the movement of the same particle material whose initial position **X** is known and tries to get the end position. The Lagrangian approach is suitable to study of the solid mechanic, which is necessary to include any constitutive equation about the behavior of the material particles.

Associated with the movement there is a second-order tensor called deformation gradient **F**, defined by

$$\mathbf{F} = \frac{\partial \phi(\mathbf{X}, t)}{\partial \mathbf{X}} = \frac{\partial \mathbf{x}}{\partial \mathbf{X}} \tag{3.17}$$

This tensor contains the information of the deformation that occurs in the environment of a point of the reference configuration X. Thus this tensor relates elements of the reference configuration and the elements of deformed configuration in the following form

$$d\mathbf{x} = \mathbf{F}d\mathbf{X} \tag{3.18}$$

The tensor **F** also relates the volume in the reference configuration and deformed configuration by its determinant at all times. The volume ratio must be greater than zero so that the predefined movement is admissible, otherwise the material will be destroyed in the deformation process.

$$J = \det(\mathbf{F}) \quad (J > 0) \tag{3.19}$$

From the deformation gradient tensor are obtained different deformation measurements such as Cauchy-Green tensor. These tensors allow to determine the elongation that suffers a fiber of a material of known initial length and whose initial orientation is given by a unit vector.

Left Cauchy-Green deformation tensor:

$$\mathbf{C} = \mathbf{F}^{\mathrm{T}}\mathbf{F} \tag{3.20}$$

Right Cauchy-Green deformation tensor:

$$\mathbf{B} = \mathbf{F}\mathbf{F}^{\mathrm{T}} \tag{3.21}$$

Green-Lagrange deformation tensor:

$$\mathbf{E} = \frac{1}{2}(\mathbf{C} - 1) \tag{3.22}$$

For stress measurement, it is assumed that there is a stress vector which is measured in the deformed configuration that is reached from the Cauchy postulate. It is also required the use of other stresses measures because of the undeformed configuration. This postulate established that the stress on a point **x** only depends on the normal to the surface at this point(**n**), so $\mathbf{t} = \mathbf{t}(\mathbf{x}, \mathbf{n})$. Based on these concepts we define the Cauchy stress tensor σ, which verifies

$$\mathbf{t}(\mathbf{x}, \mathbf{n}) = \sigma(\mathbf{x})\,\mathbf{n} \tag{3.23}$$

From σ are defined other stresses tensors such as the Piola-Kirchhoff tensors. The first Piola-Kirchhoff stress tensor provides the strength in the deformed state, but referred to the undeformed surface. It is a non-symmetric tensor.

$$\mathbf{P} = J\sigma\mathbf{F}^{-\mathrm{T}} \tag{3.24}$$

The second Piola-Kirchhoff stress tensor corresponds to the strength in the deformed state, but converted to initial state and referred to the unit area of the initial state. As can be seen in its expression, is a symmetric tensor.

$$\mathbf{S} = \mathbf{F}^{-1}\mathbf{P} \tag{3.25}$$

Once defined the tensors we introduce some of the constitutive equations for hyperelastic materials. Without internal restrictions the constitutive equation of a hyperelastic material is given by the expression

$$\mathbf{S} = \frac{\partial W}{\partial \mathbf{E}} \tag{3.26}$$

relating the energy function W and the second Piola-Kirchhoff stress tensor.

The realtion between **S** and **E** is not linear. The solution in an implicit scheme is approximated linearizing respect to variations of intantaneous configuration. For all this, it is needed a fourth-order tensor:

$$\mathbb{C} = \frac{\partial \mathbf{S}}{\partial \mathbf{E}} \tag{3.27}$$

If the material is hyperelastic equation is rewritten as

$$\mathbb{C} = \frac{\partial^2 W}{\partial \mathbf{E}\partial \mathbf{E}} = 4\frac{\partial^2 W}{\partial \mathbf{C}\partial \mathbf{C}} \tag{3.28}$$

Biofilm samples have little compressibility compared to the shear stiffness. As a result we can define the material as incompressible. This condition corresponds with the restriction $J = 1$ and the above equation is as follows

$$\mathbf{S} = 2\frac{\partial W}{\partial \mathbf{C}} - p\mathbf{C}^{-1} \tag{3.29}$$

where p is a scalar. The term on the right, which includes p, is a term that keeps the incompressibility penalty model. This equation can be considered such as the general constitutive equation of an incompressible hyperelastic material.

3.3 Biofilm Model

It is known that the EPS influence the mechanical stability of biofilms[36]. The composition and quantity of EPS formed by mycroorganisms vary and depend strongly on types of organism and various enviromental factors. As different as the composition of EPS molecules may be, the result is always a hydrogel in which the cells are embedded and which keeps the biofilm adhering to the support. Some biofilms represent very delicate structures such as developing under stagnant water conditions, while others can be extremely resistant to shear forces such as biofilms on the walls of pipes through which water runs with high velocity.

To understand these characteristics, three types of interactions must be considered which are also theoretical basis to understand the behaviours of EPS[10]:

- Dispersion(London) forces: Active over the entire molecule and not localiced in functional groups. The source of this type of interaction is the spontaneous formation of trasient dipoles due to fluctuations in the electron distribution within the molecule. These temporary dipoles will polarise neighboring molecules, thus creating dipolar attraction forces. It represents the main cohesive force between hydrocarbon chain.
- Electrostatic interactions: Active between ions, permanent and induced dipoles. The ionic interactions are relatively strong; it is mainly interactions involving divalent cations, in particular Ca and responsible for a considerable proportion of the overall binding energy. They can be influenced by ionic strength, complexing agents and by the pH-value.
- Hydrogen bonds: Mainly active between hydroxyl groups as particularly frequent in polysaccharides and water molecules.

The individual binding force of any type of these three interactions is smaller compared to a covalent C-C bond. However, the large number of functional groups of a macromolecule may result in a overall binding energy which is well in the range of several covalent C-C bonds. Polysaccharides in EPS are good examples to demonstrate this: some polysaccharides provide additional capacities for London dispersion forces. Others polysaccharides, such as alginate, display by means of their carboxylic groups many electrostatic interaction sites. They either repel each other, or are attracted to each other when are bridged by divalent cations.

As a result, the elastic and mechanical properties of biofilms can be probed studying the chain elasticity of polymers. Below it is presented a constitutive model to describe the mechanical behaviour of microbial biofilms based on classical approaches in the continuum theory of polymer networks[5]. The model is a network of extracellular polymeric substances and can be described as a superposition of worm-like chain networks, each

connected by transient junctions of a certain lifetime.

Quantitative information regarding chain elasticity can be obtained using statistical mechanical, random walk formulations, that is, the freely jointed chain(FJC), the wormlike chain(WLC), the extensible FJC, or the extensible WLC model. This study begin with WLC model, which it was modelled the mechanical behavior of biofilms and which is programmed the subroutine and used in the simulations.

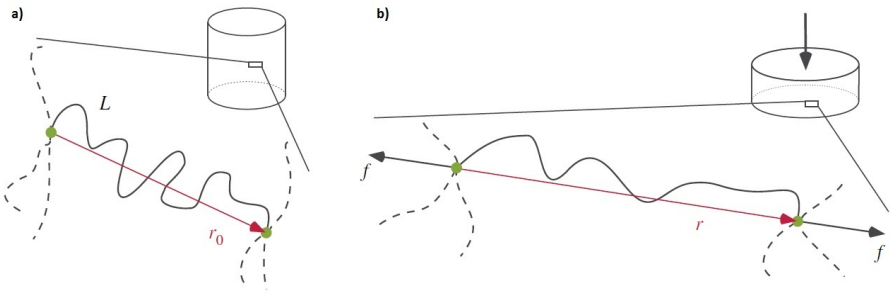

Figure 3.8: a) Reference state of a worm-like chain(WLC) of contour lenght L; b) Force f applied on the chain ends, which variates the end-to-end distance from r_0 to r. (Ehret,2012)[5]

In the WLC model the polymer chain is considered to be continuously curved and the direction of the curvature at any point in the chain is random. The chain in this model is intermediate between a rigid rod and a flexible coil. The WLC model takes into account the local stiffness of the chain in terms of the persistence length(l_p) and its contour length(L), i.e. its fully extended length[5]. The force required to stretch a wormlike chain in a solvent to its end-to-end distance r, supplemented by eight-order polynomial is given by

$$f(r) = \frac{k_\mathrm{B}\Theta}{4l_\mathrm{p}}\left[\frac{1}{(1-r/L)^2} - 1 + 4\frac{r}{L} - 3\left(\frac{r}{L}\right)^2\right] \tag{3.30}$$

where $0 \leq r < L$, $k_\mathrm{B} = 1.381 \cdot 10^{-23} JK^{-1}$ denotes Boltzmann's constant and Θ stands for the absolute temperature.

The strain energy function of the corresponding eight-chain model is calculated in terms of the first principal invariant of the right Cauchy-Green tensor $I_1 = \mathrm{tr}(\mathbf{C})$ as

$$\lambda = \frac{r}{r_0} = \sqrt{\frac{I_1}{3}} \tag{3.31}$$

Apart from that, it is introduced in the strain energy function the ratios $\Lambda = r_0/L$ and $\Omega = L/l_\mathrm{p}$. It is also introduced one factor n_i that represents the number of chains per

unit reference volume. This chains will be assumed to be inextensibe and the network incompressible, which this condition implies a restriction in the determinant of the deformation gradient $\mathbf{F}$, that $\det(\mathbf{F}) = 1$, as already explained in the previous section.

It is assumed that in the EPS matrix from a biofilm are present four former connetion mechanisms, the first three, previously explained, derived of the electrostatic interactions and hydrogen bonds. Last one derived from the presence of entanglements in the EPS matrix. Therefore it is necessary derive the strain energy of a network with four different types of junctions as

$$W = \sum_{i=1}^{4} W_i + W_0 \tag{3.32}$$

$$W_i = \frac{k_B \Theta}{4} n_i \Omega_i \left\{ \frac{1}{1 - \Lambda_1 \sqrt{I_1/3}} - \Lambda_i \left[\sqrt{\frac{I_1}{3}} - 2\Lambda_i \frac{I_1}{3} + \Lambda_i^2 \left(\frac{I_1}{3} \right)^{3/2} \right] \right\} \tag{3.33}$$

where W_0 is a constant term that guarantees zero strain energy in the reference state. According to the second Piola-Kirchhof stress tensor $\mathbf{S}$ in cosideration of the incompressibility[37], as already explained in the previous section

$$\mathbf{S} = 2\frac{\partial W}{\partial \mathbf{C}} - p\mathbf{C}^{-1} = \sum_{i=1}^{4} 2\frac{\partial W_i}{\partial \mathbf{C}} - p\mathbf{C}^{-1} = \sum_{i=1}^{4} 2n_i g_i \mathbf{I} - p\mathbf{C}^{-1} \tag{3.34}$$

where $\mathbf{I}$ is the indetity tensor of second order, p denotes the arbitrary hydrostatic pressure and $g_i = \hat{g}_i(I_1) = n_i^{-1} \partial W_i / \partial I_1$ represent response functions in terms of the first principal invariant.

The rate of breaking of any set of chains is characterized by n_i as

$$\frac{dn_i}{dt} = -\frac{1}{T_i} n_i \tag{3.35}$$

where T_i is a constant that characterizes the lifetime of a junction[38].

It is defined that the deformation suffered by a chain depends by two defined times. The first one, time t, is the current time and the second one is the time s at which the junction is formed where $s \leq t$. The deformation suffered by a chain is expressed by the relative deformation gradient between the times s and t:

$$\mathbf{F}_*(t, s) = \mathbf{F}(t)\, \mathbf{F}^{-1}(s) \tag{3.36}$$

With this and the definition $\mathbf{C}^{-1}(s) = \mathbf{F}^{-1}(s)\,\mathbf{F}^{-\mathrm{T}}(s)$ in question, it is finded the invariant

$$I_* = \mathrm{tr}(\mathbf{F}_*^{\mathrm{T}}\mathbf{F}_*) = \mathbf{C}(t) : \mathbf{C}^{-1}(s) \tag{3.37}$$

where the colon indicates the scalar product of two second-order tensor.

The stress $\mathbf{S}_i$ at time t results from integration over the complete history as

$$\mathbf{S}_i(t) = \int_{-\infty}^{t} M_i(t-s)\, 2\hat{g}_i(I)\, \mathbf{C}^{-1}(s)\, \mathrm{d}s \tag{3.38}$$

where the memory function $M_i(t-s) = T_i^{-1} e^{-(t-s)/T_i}$ has been introduced.

This integral expression takes the form of a particular K-BKZ equation in Lagrangian description[39]. According to the second Piola-Kirchhof stress tensor it is deduced the Cauchy stress tensor for the viscoelastic material, which describes the EPS network of a biofilm as

$$\boldsymbol{\sigma}(t) = J(t)^{-1} \sum_{i=1}^{4} \int_{-\infty}^{t} M_i(t-s)\, 2\hat{g}_i(I) \times \mathbf{F}(t)\, \mathbf{C}^{-1}(s)\, \mathbf{F}^{\mathrm{T}}(t)\, \mathrm{d}s - p\mathbf{I} \tag{3.39}$$

4 Biofilms Rheology

4.1 Rheological Basis

Rheology is a scientific discipline which is dedicated to the study of deformation and flow of materials, specifically, the study of the fluids. The word rheology comes from Greek $\rho\epsilon\iota\upsilon$, which means flow.

Although rheology may cover everything that is related to the flow behaviour in aeronautics, fluid mechanics and including solid mechanics. The aim of rheology is limited to the observation of the material behaviour under very soft deformation. Through the observation and knowledge of the strain field applied, in many cases, the rheologist can develop a constitutive or mathematical model to obtain the functions that characterize materials or the material properties.

The material functions and constitutive relations have several uses in practice, depending on the purpose of the study in each type of material. Regarding this, we can distinguish two main objectives:

- Predict the macroscopic behaviour of the fluid under process conditions using the constitutive relations and functions of materials.
- An indirect study of the microstructure of the fluid and evaluate the effect of various factors on that microstructure. For that, material functions are compared with rheological properties.

Fluids studied in Rheology have a spectrum of behaviours in range from the Newtonian viscous liquid until Hooke elastic solid. To introduce these techniques we will discuss briefly the creep-recovery test carried out on the three rheological models that have been previously described in section 3.1.

On the creep test an effort is instantaneously applied and mantained constant for a certain period of time, and then is suddenly recalled. The strain which is produced in the sample is recorded during the time while the stress is applied. Then in the next period of time we show the recovery of the deformation which tends to reach the steady state that it had before applying stress.

If the creep test is performed considering **the Kelvin-Voigt model**(spring and dashpot in parallel), the result is the behaviour that is illustrated in the next figure. Furthermore,

after releasing the stress, deformation is not recovered until the delay time is finished. This behaviour is similar to a solid, it reaches a maximum strain and a full recovery. The difference is the liquid behaviour that it has, which requires some period of time until the recovery state.

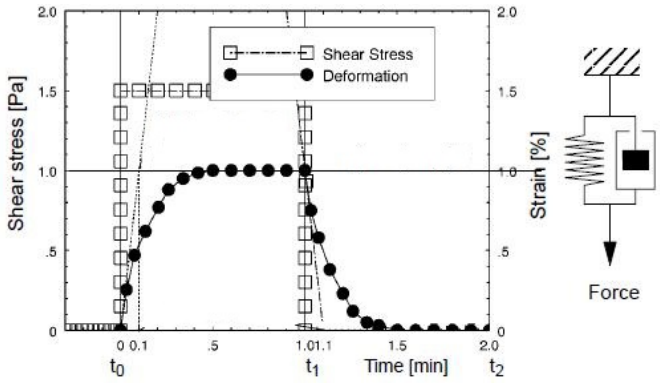

Figure 4.1: Creep and recovery of a Voigt's solid versus time. Strained sample can relax while the stress is maintained and when the stress is removed the recovery of the strain is retarded. (Schramm,2004)[3]

The behaviour obtained assuming **the Maxwell model**(spring and dashpot in series) is shown in the following figure. In this case, the behaviour is closer to a liquid than a solid, that is generally used by the term the Maxwell fluid. In short periods of times the elastic response occurs immediately, while in long periods of time, greater than the relaxation time, it follows a single viscous behaviour.

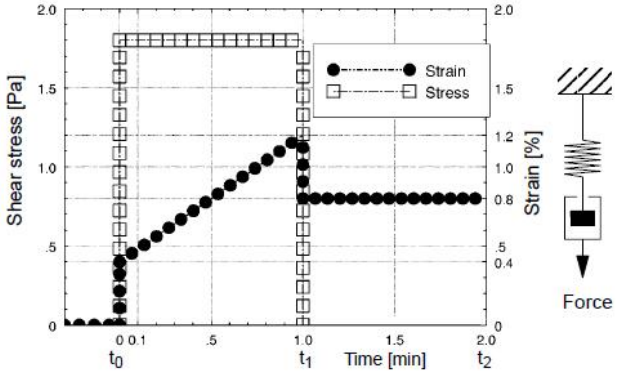

Figure 4.2: Creep and recovery of a Maxwell's liquid versus time. This model reacts first with an instantaneous step of strain increase and in later phase of the test shows a viscous response. Removed the applied stress, the strain drops immediately to a constant level. (Schramm,2004)[3]

Finally, we can represent the most complex case, in which four constants are used. This is given by **the Burger's model**, resulting from the series combination of a Kelvin-Voigt's model element in series with a Maxwell's model which is illustrated schematically below. Applying a stress, an elastic deformation occurs instantaneously, but the strain rate decreases until a certain time. Finally, the steady flow is reached.

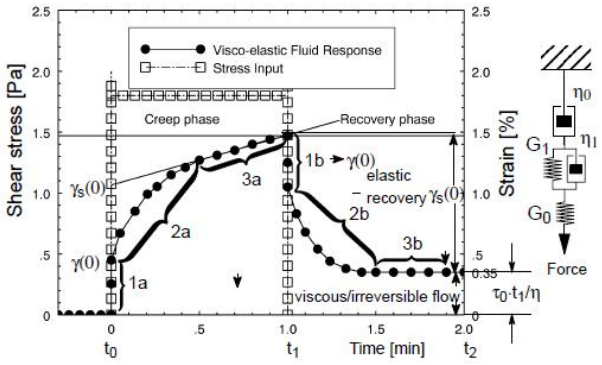

Figure 4.3: Creep and recovery of a Burger's model as a function of time. 1a) instantaneous strain step; 2a) gradual increase of the strain curve; 3a) purely viscous response; 1b) instantaneous strain reduction; 3b) non-recovered viscous flow; 2b) irreversible strain constant level. (Schramm,2004)[3]

This way, three regions can be established similar to the recovery phase. The amount of deformation that is recovered is called recoverable shear strain in steady flow. When the stress is not very high(linear viscoelasticity limit), the deformation at any time is equal to the sum of the deformation recoverable and non-recoverable deformation.

4.2 Oscillation Test

Using the dynamic test is possible to characterize the viscosity and elasticity according to the response time, relating the angular velocity or the frequency with the oscillation stress or strain[40]. It is a small deformation test, widely used to evaluate the response of complex fluids in the linear viscoelastic region, applying a low-amplitude oscillatory shear.

Applying a sinusoidal deformation (γ), the equation which describes the elastic response is

$$\gamma = \gamma_0 \sin(\omega t) \tag{4.1}$$

where γ_0 is the maximum deflection, ω the angular velocity ,$\omega = 2\pi f$ and t the time.

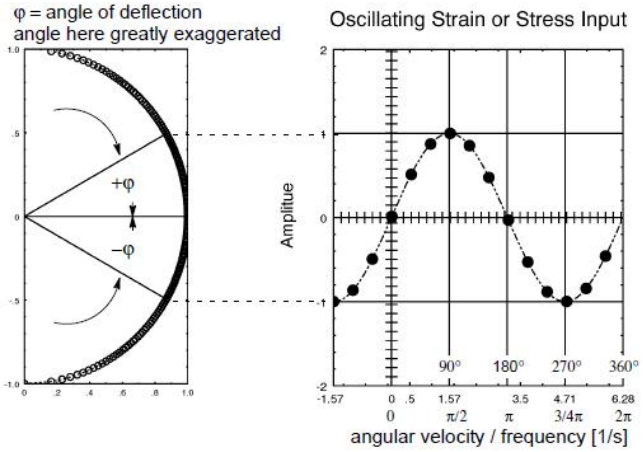

Figure 4.4: Dynamic oscillation test. Rotational rheometer is made to deflect with sinusiodal time-function alternatively for a small angle φ to the left and to the right. This test mode relates the assigned angular velocity or frequency to the resulting oscillating stress or strain. (Schramm,2004)[3]

This equation defines the function of stress which, for an ideal solid, it would be formed as:

$$\tau = G\gamma_0 \sin(\omega t) \tag{4.2}$$

According to these equations, the strain and stress are in phase. However, the response of an ideal fluid (viscose) is given by:

$$\tau = \eta\dot{\gamma} = \eta\omega\gamma_0 \cos(\omega t) \tag{4.3}$$

where the strain and stress are offset at an angle $\delta = 90°$, therefore it can be rewritten the previous equation as:

$$\tau = \eta\omega\gamma_0 \sin(\omega t) \tag{4.4}$$

A viscoelastic fluid is characterized by an intermediate phase angle between $0°$ (elastic) and $90°$ (viscous). On a dynamic test in the CR measured mode, deformation is assigned to an amplitude and an angular velocity. The resulting stress (τ) is measured with the stress amplitude (τ_0) and the phase angle (δ):

$$\tau = \tau_0 \sin(\omega t + \delta) \tag{4.5}$$

In rheology is often used the term **complex modulus** (G^*), which is given by:

$$G^* = \frac{\tau_0}{\gamma_0} \tag{4.6}$$

It represents the total resistance of a substance to the applied stress. Due to the fact that G^* and τ depend on the frequency, it is necessary to carry out a frequency sweep to determine the linear viscoelastic region, in which the viscosity and elasticity do not change with increasing stress amplitude.

Using trigonometry, it is established

$$\tan\delta = \frac{\tau_0^{''}}{\tau_0^{'}} \tag{4.7}$$

in which $\tan\delta$ is called **loss tangent**. This decomposition suggests two dynamic modules related to the phase angle. $\tau_0^{'}$ represents the shear stress amplitude related to the elastic modulus and $\tau_0^{''}$ represents the shear stress amplitude related to the viscous modulus.

Thus, G' would be a phase modulus, and G'' would be an out of phase modulus:

$$G^{'} = \frac{\tau_0^{'}}{\gamma_0} \tag{4.8}$$

$$G^{''} = \frac{\tau_0^{''}}{\gamma_0} \tag{4.9}$$

Therefore, it can be rewritten as

$$\tan\delta = \frac{G^{''}}{G^{'}} \tag{4.10}$$

The previous notation comes from the imaginary number, where it is known

$$\mathrm{e}^{i\theta} = \cos\theta + i\sin\theta \tag{4.11}$$

Therefore, it can defined the complex modulus G^*, constituted by a real part ($G^{'}$) and an imaginary part ($G^{''}$)[3]:

$$G^* = G^{'} + iG^{''} \tag{4.12}$$

or which is the same,

$$\tau = G^{'}\gamma_0 \sin(\omega t) + G^{''}\gamma_0 \cos(\omega t) \tag{4.13}$$

Finally, the equations that define each of the components are:

$$G^{'} = G^{*}\cos\delta = \frac{\tau_0}{\gamma_0}\cos\delta \tag{4.14}$$

$$G^{''} = G^{*}\sin\delta = \frac{\tau_0}{\gamma_0}\sin\delta \tag{4.15}$$

where $G^{'}$ is called **elastic modulus** or **storage modulus** because it indicates that the energy supplied by the stress is temporarily stored during the test. But this can be recovered once the stress is released, i.e. there is elastic recovery. Moreover, modulus $G^{''}$ is called the **loss modulus** because this term is associated with the energy that has been used to start the flow and the irreversible loses which are transformed into heat.

The equations 4.14 and 4.15 define the materials located between the both extreme of the material behaviour, elastic or viscous pure. The viscoelastic materials or fluids are located in the range of phase angle δ, between $0°$ and $90°$.

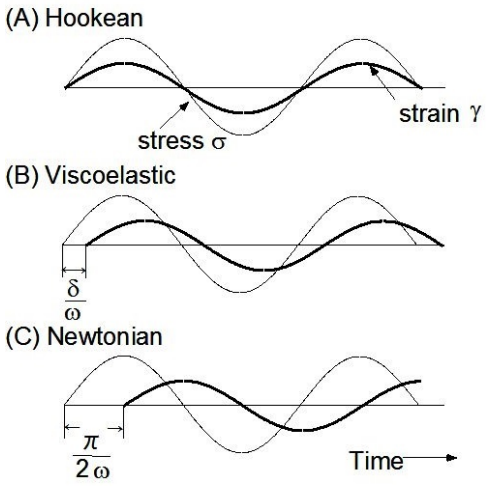

Figure 4.5: a) Hookean solid response where the strain and stress are in phase; b) Viscoelastic response where the range of phase δ are located between $0°$ and $90°$; c) Newton liquid response where the strain and stress are out of phase. (Schramm,2004)[3]

The response to the simplest combination of a spring and a dashpot in series(Maxwell's model) shows a complex behaviour at a certain frequency range, which can be expressed

mathematically with the following equations[41], where $\lambda = \eta/G$ is the relaxation time.

$$G' = \frac{\eta\omega}{1+(\omega\lambda)^2} \tag{4.16}$$

$$G'' = \frac{G^*(\omega\lambda)^2}{1+(\omega\lambda)^2} \tag{4.17}$$

Note that the complex modulus and the phase angle are frequency dependent. Therefore, to obtain the viscoelastic behaviour of the material it is needed to maintain the stress fixed and to perform the test in a range of frequencies. This result shows both curves of G' and G'' versus frequency.

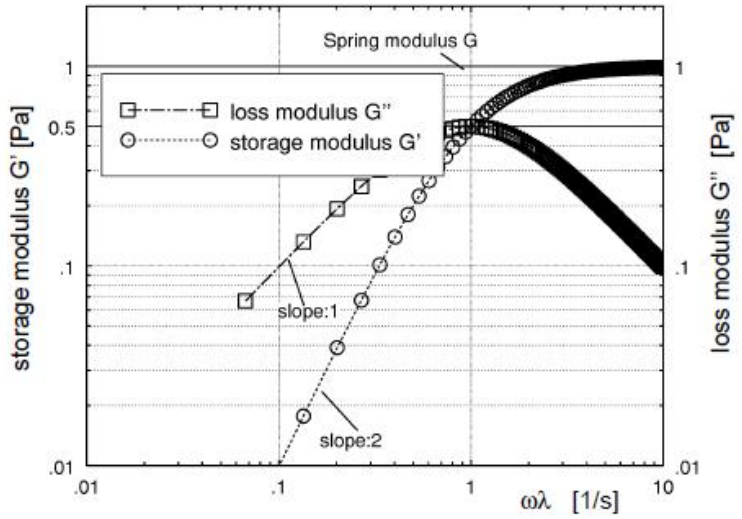

Figure 4.6: Frequency-sweep of Maxwell's model between 0.1 and 10 Hz. At low frequency the Maxwell's model reacts just as a Newtonian liquid, since the dashpot response allows enough time to react to a given strain. At high frequencies the liquid model just reacts as a single spring and the dashpot cannot react in line with the assigned strain. (Schramm,2004)[3]

In figure 4.6 is observed that in low frequencies G'' is higher than G', so predominate the viscous behaviour of a liquid. As frequency increases, the curves of G' and G'' intersect and begins to dominate the typical behaviour of a elastic solid. The value that determines which kind of behaviour is more significant is the frequency (ω) in relation to the relaxation time (λ). So, this way it is defined the **Deborah's number**, as $\omega\lambda$. If this value is low, the response is similar to a liquid, and if it is high the response will be similar to a solid material.

It is said that the linear viscoelastic region is defined by the range of efforts in which G^* remains constant and does not depend on other rheological parameters, as could be the stress or strain. The equations that quantify the linear viscoelasticity are linear differential equations and the differential coefficients are time dependent constant. This means that the values only depend on the material or suspension. Beyond the linear viscoelastic region, higher amplitudes(more effort) mean cumulative deviations of the measured data. In these conditions the sample is deformed until the temporary bonds between the molecules or aggregates are destroyed, getting in the flow zone.

For this reason, measurement of the viscoelastic behavior of a material is usually done in two stages. In a first step it is proceeded to determine the linear viscoelastic region. Once this is done, it is determined the viscoelastic modules variation in function of frequency in conditions that assure that tests are carrying out in the linear viscoelastic region.

To determine the limit between the linear region and the nonlinear viscoelastic region it is necessary to carry out dynamic tests at a certain value doing **the stress sweep**. This way the amplitude increases automatically as long as the data acquired are sufficient to perform a good correlation between the strain and stress. Accordingly, once it is obtained an amplitude curve versus G^* or stress, it can be clearly shown if the sample contains elastic region or not. Additionally, this type of charts show that $G^{'}$ normally decreases faster than $G^{''}$, which may increase before declining.

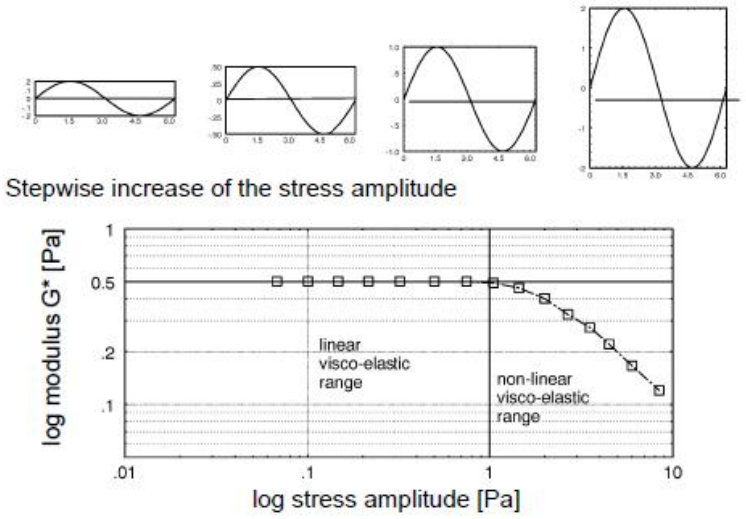

Figure 4.7: Stress amplitude sweep. In this diagram the complex modulus G^* curve runs parallel to the abscissa, linear range, until this curve starts to break away from the constant level, non-linear range. The linear viscoelastic range is limited to that amplitude range for which G^* is constant. (Schramm,2004)[3]

Once the linear region is known, it proceeds to a second type of test: **the frequency**

sweep. In this case, a constant stress or strain is applied(within the linear region) and the response of the material in a range of frequencies is studied, which allows to represent the elastic and viscous modulus and the phase angle versus frequency, as illustrated.

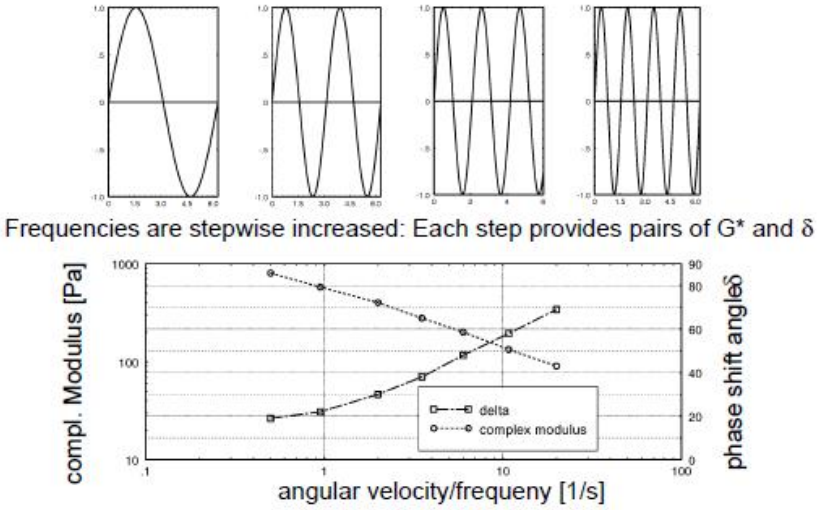

Figure 4.8: Angular velocity/Frequency sweep. The strain frequency is stepwise increased and at any frequency step the two resulting values of G^* and δ are measured. These data must still be transformed into the viscous and the elastic components of the viscoelastic behaviour of the sample. (Schramm,2004)[3]

The versatility of the current equipment can measure oscillation relatively easily and with precision. This has led to test these measures even to make determinations that can be made by simple direct methods which are faster.

4.3 Rotational Rheometer

Rotational rheometers consist basically in two parts that are separated by the fluid that is studied. These parts can be two cylinders, two parallel surfaces, one surface and a small cone angle, a rotor inside a cylinder... The movement of these parts causes the appearance of a velocity gradient along the fluid. The viscosity of the fluid can be determined by measuring the effort required to produce a certain angular velocity. These viscometers are more versatile and can be used for non-Newtonian fluids.

The rheometer measures the resistance to oscillation and the delay of the resistance. As it is already explained in the viscoelasticity theory in section 4.2, an ideal elastic solid does not present delay, while a perfect viscous liquid presents a phase delay of $90°$. Viscoelastic materials generally present phase angle between $0°$ and $90°$ degrees.

A rheometer with this feature operates applying a sinusoidal strain, so that no information is generated on shear rate but gives us information about the frequency in terms of radians per second. The computer which is connected with the rheometer may qualify the viscous nature, known as the loss modulus G'' and the nature of the gel, known as elastic or storage modulus G'. The instrument also determines the vector sum of these two components, called complex modulus G^*.

Rotational measurements fall into one of two categories[42]: **stress-controlled** or **rate-controlled**.

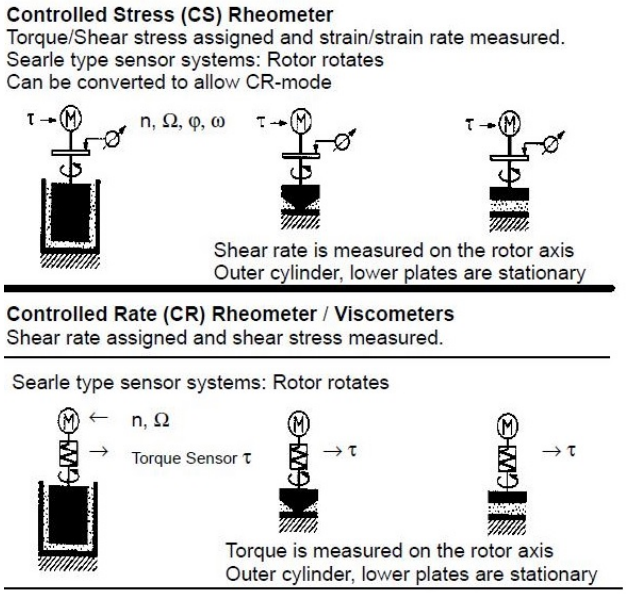

Figure 4.9: Concentric cylinder, cone-plate and plate-plate rheometer in Controlled Stress(CS) or Controlled Rate(CR) mode. In CS mode it is applied torque and measured shear strain. In CR mode it is applied shear strain and measured torque. (Schramm,2004)[3]

In **stress-controlled(CS)** rheometers set a determined effort(the torque applied by the rotor on the sample) and measure the shear rate corresponding to this pair. It is always better to use a CS rheometer to evaluate the processes controlled by effort, such as processes in which there is a compression of the sample, or that the flow conditions are generated by gravitational forces, sedimentation, drip paintings, etc.

In **rate-controlled(RC)** rheometers fixed the shear rate and measured the effort on the torque generated. It is always better to use a RC rheometer to evaluate processes controlled by the rate of shear, for example under flow conditions that are imposed by external means, such as pumps, mixers, spray, etc.

Another rheometers classification is according to the type of tooling used in the measurements. It is described the three most commonly used types of rheometers which are: **concentric cylinder rheometer**, **cone-plate rheometer** and **plate-plate rheometer**.

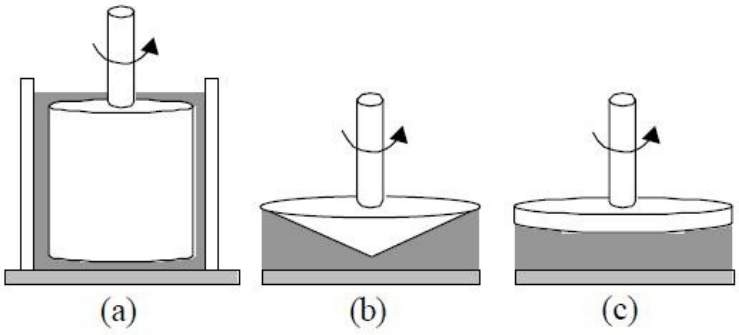

Figure 4.10: Three possible geometrical configurations in rotational rheometers: a) Concentric Cylinder; b) Cone-Plate; c) Plate-Plate. (Bohlin,2001)[6]

The **concentric cylinder rheometer** was the first rheometer which has been used. It consists of two concentric cylinders, an outer and an inner hollow solid (in English literature can be found as "cup and bob"). The movement of the cylinders generates shear in the annular space of the liquid.

These instruments can perform measurements in two ways: the first one, rotating one of the elements with a certain torque and measuring the rotational speed generated. The second way, generating a rotational speed in one of elements and the measuring the opposite torque. Both methods were already studied before the Second World War, and its fundamentals were introduced by Couette in 1888, in whose honor, the flow caused between concentric cylinders is called Couette flow.

The **cone-plate rheometer** is based on the shear present in a fluid situated in the space between a cone and a plate. The angle between them must be very small (less than $4°$, considering that with high angles, the calculations will be more complicated). If the cone rotates with a certain angular velocity, ω, it causes a rotational movement in the fluid so that it rotates at a higher rate near the walls of the cone.

All cone-plate instruments allow cone extraction for changing the sample, which facilitates cleaning in many cases. This last advantage and the small quantity of sample required, are the major advantages that this type of equipment represents. In most rotational rheometers shear rate changes related with distance from the center of rotation. However, in the cone-plate rheometer the shear rate along the cone spacing is constant because the gap between the cone and plate increases while the distance incresases from

the center. Non-Newtonian fluids do not need to carry out corrections, being possible to apply the equations for Newtonian fluids.

In the **plate-plate rheometer** the fluid is set between two parallel plates, the upper turns and the lower is immobile. The fluid elements near the mobile plate have a higher speed than those which are found near the fixed plate. Thus, the shear stress is produced from the bottom to the top of the plate.

As in the cone-plate viscometers, these instruments are easy to clean and require small amounts of sample. The ability to set the thickness of sample (gap) according to the characteristics of the same is an advantage in suspensions of large particles or liquids that tend to be ejected outside the plates. However, the viscosity of the sample is difficult to evaluate because the shear rate changes according to the distance from the center of the plate.

4.4 Plate-Plate CS-Bohlin Rheometer

The following information is based around the Bohlin range of rheometers and viscometers but should be equally applicable to other instruments which have similar configurations[6]. In our case, the rheometer that has been used in the tests was the CS-Bohlin Rheometer.

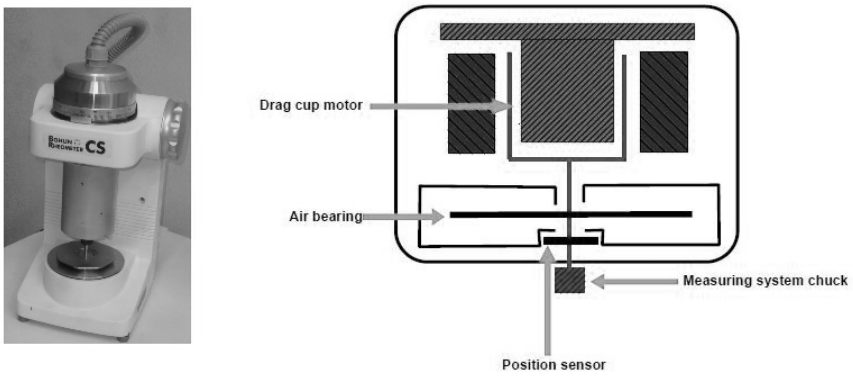

Figure 4.11: Bohlin CS-Rheometer used in IBVT biotechnology institute to test biofilm samples. The principal components of a CS Rheometer are shown in the picture. The rheometer is a constant torque motor which works by a drag cup system. An angular position sensor detects the movement of the measuring system attached to the shaft. (Bohlin,2001)[6]

The software automatically converts the applied value of torque to a shear stress when the data is displayed. The data from the position sensor is converted to a strain, again using the information about the current measuring system. Monitoring the change of

strain as a function of time it is obtained the shear rate.

Due to the fact that the only data which is produced by the rheometer is a deflection reading (from the angular position sensor), the maximum shear rate you can achieve is determined by the time you are prepared to wait. The sensor must turn a measurable amount for the software to calculate a speed and hence a shear rate.

Rheometers and viscometers work with torque and angular velocity. It is normally used shear stress and shear rates, so then is necessary the use of a method to convert from 'instrument numbers' to 'rheology numbers'. Each measuring system used in an instrument will have its associated 'form factors' to convert torque to shear stress and angular velocity to shear rate.

Shear rates and shear stresses are mathematically defined for parallel-plate sensor system by Thermo Haake Rheology[3]. It is determined by the plate radius R and the distance h between the plates.

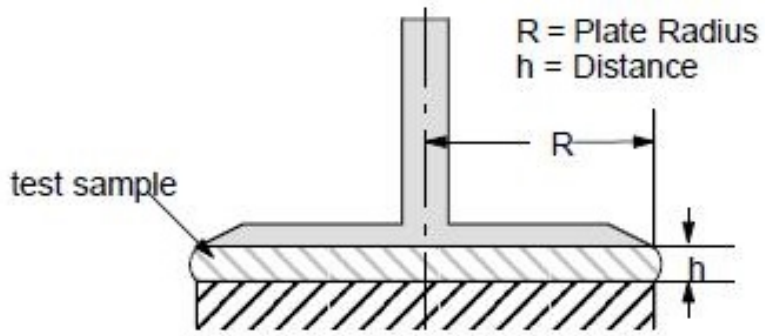

Figure 4.12: Plate-plate rheometer geometry. Parallel plate geometries are referred to by the diameter of the upper plate. for instance a PP40 is a 40mm diameter plate. The lower plate is either larger than or the same size as the upper plate. (Schramm,2004)[3]

This distance can be varied, but it should be not smaller than 0.3mm and not larger than 3mm. Otherwise sizeable measuring errors related to the nature of the sample cannot be avoided. Parallel-plate senor systems are chosen instead of cone-and-plate sensor system if samples containing larger filler particles. The chosen gap should be at least 3 times larger than the biggest particle size.

Shear Rate (γ_0): The shear rate of this system is dependent on the specific radius r of the plates: $0 < r < R$. The shear rate given for such a sensor system is calculated for the outer radius R. For the viscosity measurement of Newtonian liquids it does not matter that this sensor system is not characterized by a single shear rate, but for a wide shear rate

range from zero at the plate center and high at R. For non-Newtonian fluids the shear stress must be corrected:

$$\dot{\gamma}_{\text{max}} = M\Omega \, [1/\text{s}] \tag{4.18}$$

$$M = \text{Geometric factor} = R/h$$
$$R = \text{Outer radius} \, [\text{m}]$$
$$h = \text{Gap size between plates} \, [\text{m}]$$
$$\Omega = 2\pi n/60 \text{ whereby } n = \text{ rotor speed } \left[\text{min}^{-1}\right]$$

Deformation (γ): It relates the geometry of the sensor system with the angular deflection.

$$\gamma = M\varphi \tag{4.19}$$

$$M = \text{Geometric factor} = R/h$$
$$\varphi = \text{Deflection angle} \, [\text{rad}]$$

Shear Stress (τ): The shear stress at the outer edge of the plate is proportional to the torque M_{d} and the geometry factor A.

$$\tau = M_{\text{d}} A \, [\text{Pa}] \tag{4.20}$$

$$A = 2/\pi R^3$$
$$R = \text{Outer radius} \, [\text{m}]$$

In fluids which show a non-Newtonian flow behaviour (power-law-exponent $n < 1$) the shear stress must be corrected according to Weissenberg:

$$\tau = M_{\text{d}} A \left(\frac{3+n}{4}\right) [\text{Pa}] \tag{4.21}$$

As it is already mentioned the shear stress varies across the radius for a parallel plate. For Bohlin CS-Rheometer the shear rate given for such a sensor system is calculated in reference to the $3/4$ radius position if the test sample is Newtonian. This way the above equations are rewritten as:

Shear Rate (γ_0)

$$\dot{\gamma}_{\text{max}} = M_1 \Omega \, [1/\text{s}] \tag{4.22}$$

$$M_1 = \text{Geometric factor} = 3R/4$$
$$R = \text{Outer radius} \, [\text{m}]$$

Shear Stress (τ)

$$\tau = M_\text{d} M_2 \, [\text{Pa}] \tag{4.23}$$

$$M_2 = 3/2\pi R^3$$
$$R = \text{Outer radius} \, [\text{m}]$$

5 Modelling Experiment

5.1 Ibvt Test

5.1.1 Rheological Characterization of Hydrogels

The focus of this work[11] is to establish hydrogel as a model of biofilm. Biofilms have an EPS matrix and show a reversible deformation similar to hydrogels. For this purpose, a suitable hydrogel was identified, which imitates the physicochemical properties of biofilms.

The study examined the rheological behaviour of hydrogels such as the complex shear modulus, the storage modulus and the complex viscosity. Other properties, such as the viscous and elastic resilience may be calculated from the known relationships. Moreover, the effect of divalent cations such as Mg and Ca was checked on the gel strength. Finally the *Pseudomonas Putida KT2440* cells were immobilized within the gel to simulate the biofilm's behaviour under mechanical stress.

The viscoelastic behaviour can be described by means of a plurality of models which consist in the combinations of damper and spring. In this work, an adaptation of the Maxwell material for the gel with 1% gellan, 0.05 M NaCl and 0.025 M Mg was made.

In an amplitude sweep a verification of the linear viscoelastic region was performed to ensure the validity of the mathematical relationships. The measurements at a constant deformation of 1% and in a frequency range of 0.1 to 10 Hz enabled the determination of the viscoelastic parameters such as the complex shear modulus, the storage modulus and the loss modulus.

The averaged values of the modules over the replicas were plotted on the frequency, in order to show the various modules of the gel composition, which are of the order of 4000-8000 Pa. With these findings, it was possible to create a model using the CCD. With this model we could predict the shear modulus at a frequency of 1 Hz.

The experiments at a constant stress of 50 Pa and a constant frequency of 1 Hz were not conducted edge-free. The complex shear modules are up to eight times larger than the modules of the edge-free experiments. This difference is caused by the adhesive forces which are formed between the material and the shell.

The influence of the divalent cations in the gel strength was tested. It has been shown

that Ca cations has a greater impact on the gel hardness than Mg.

In the last test, which we will discuss in detail below, the hydrogel was immobilized with *Pseudomonas Putida KT2440* cells. The curve of the storage modulus is not constant with increasing frequency. It also shows a sharp increase at high frequencies. The loss modulus is constant at low frequencies but it decreases at high frequencies. Without cells in the gel, the storage modulus is higher than the loss modulus. However in gels with *P. Putida*, the loss modulus exceeds at low frequencies the memory modulus.

5.1.2 Description of the Tests

The tests that have been performed in this work were carried out according to two configurations. The first configuration was set up for testing frequency and constant efforts. The second configuration for frequency sweep tests.

Non-Free-Edge Sample: Amplitude-Sweep. In this mode it is possible to determine the linear viscoelastic region of the sample. The test was carried out with a force sensor in the following mode:

- Frequency: 1 Hz
- Shear stress: 50 Pa
- Logarithmic strain delay: 3 sec

About the sample geometry and rheometer tools used in these tests:

- Upper plate: Bohlin plate. 40mm diameter
- Lower plate: Petri dish with Gel. 60mm diameter

The upper plate of the rheometer pushes always with the same force on the gel (about 2 N). This force was determined by the force sensor, which was attached to the lower plate.

Free-Edge Sample: Frequency-Sweep. This mode enables the investigation of the viscoelastic properties as a function of frequency always working in the linear viscoelastic region:

- Minimum Frequency: 0.1 Hz
- Maximum Frequency: 10 Hz
- Deformation: 0.01 (referred to sample height)

- Logarithmic strain delay: 5 sec

About the sample geometry and rheometer tools used in these tests:

- Upper plate: Bohlin plate. 40mm diameter
- Lower plate: Bohlin plate. 40mm diameter
- Hydrogel Height: 1.3-1.75mm

Concerning the determination of the height gap, this could have been determined using a caliper or with a camera. The measurement with the camera is advantageous because this way the gap can be determined after the shutdown of the upper plate, and just before the start of measurement.

5.1.3 *P.Putida KT2440* Frequency Test

To simulate the effect of the cells in a biofilm of *P. Putida*, cells were immobilized in the gel. The effect of the embedded cells on the rheological properties of the gel was also determined rheologically. Furthermore, the influence of the percentage of wet biomass in the gel was considered.

These tests were performed applying the frequency sweep test and using a free-edge sample. This configuration is as described in the previous section. Measurements have been made for various wet biomass concentrations(3.2% and 4.5%) and different gel compositions. Our study is focused on the central gel composition described in the study based on gellan.

The gels, without the immobilized cells, have substantially lower loss modules. The storage modulus is greater by a factor of 10 to 20 to the loss modulus. In this case the modules are located next to each other and the factor is reduced to 3-4. This means that the properties of the gel are not only elastic but also viscous. The gel is stronger by embedding the cells but loses the ability to evade the forces flowing through, and to reduce stress.

The proportion of wet biomass shows a significant influence on the size of the modules. The storage modulus and loss modulus are higher for the gel with more embedded cells. There may be a relationship between the values of shear stress, storage modulus and loss modulus for both concentrations of wet biomass formed in gel.

In reference to the results it can be observed that the curves of the gels that are run without immobilized cells is substantially flat. The results which represent the storage modulus, reflect a higher magnification with increasing frequency. The loss modulus of the gels with embedded cells is substantially greater than in gels with no cells. Thus, the

immobilized cells have a strong influence on the gel strength.

It is also noted that the curves of storage modulus and the loss modulus show behaviour close to Maxwell's rheological model. However generated curves are flatter and memory modulus does not reach its maximum. It can be assumed that by increasing frequency up to 100 Hz, the storage modulus can reach its maximum.

5.2 ABAQUS FEM

5.2.1 Finite Element Method

The Finite Element Method(FEM) is currently one of the most powerful tools used for the numerical resolution of a wide range of engineering problems. This method is applied in a wide variety of problems, such as structural analysis, mechanical performance of automobiles, heat transfer problems, electromagnetic, etc.

Through the Finite Element Method an approximation is performed in order to obtain the solution of continuous problems, based on the transformation of a continous body into an approximately discrete model. This transformation is called the model discretization. The continuous body is divided into a finite number of components called elements. Material properties and constitutive equations are considered in those elements, which have some characteristical points called nodes. These nodes are points of attachment of each element with its adjacent.

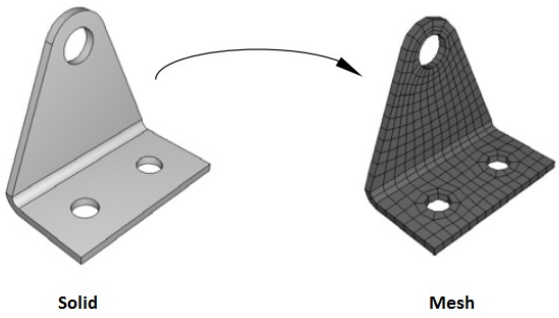

Figure 5.1: Discretization of a continous body. The body is divided into a finite number of elements. Each one of the mesh junction points are called nodes which are defined at all loads and constraints.

The behavior within each element is defined by the behavior of the nodes using the "interpolation functions" or "shape functions". These functions uniquely define the displacement field within each finite element, expressed in terms of the nodal displacements

of the respective element. Therefore, an approximation of the function values based on the knowledge of a determined and finite number of points is carried out. Although the actual shape functions are unknown, the assumption that the approximate expression can be obtained in polynomial form can be accepted.

The relation between these elements, considering the boundary conditions (loads and restrictions), leads to a system of equations whose solution will us allow to obtain results through which the approximate behavior continuous body will be known.

The Finite Element Method(FEM) can be divided into three stages:

Preprocessing. Preparation of the model to be calculated. At this stage the following operations are performed:

- Drawing of the model geometry.
- Selection of material properties.
- Application of external loads and boundary conditions.
- Discretization of the finite element model.

Resolution. Stage in which all calculations are performed and the solutions are generated. The following operations are performed:

- Selection of the type of computation to perform.
- Configuration of the calculation parameters, time intervals and number of iterations.
- Transferal of loads to the model, generation of shape functions, assembly of the stiffness matrix, resolution of equational systems obtaining the solution.

Postprocessing. In this stage the graphical representation of the results is made and the indirect results operating the solutions of the model are obtained.

5.2.2 ABAQUS Software

ABAQUS is a software that uses an analysis code by the Finite Element Method of general purpose, aimed at solving nonlinear problems. It was developed for over 20 years ago by the company Hibbit, Karlsson & Sorensen, Inc. (HKS), and is currently used to solve large and complex engineering problems[43]. ABAQUS can be used to solve problems of strength of materials, fracture mechanics, metal forming processes, heat transfer, etc.

ABAQUS is structured in three sections, corresponding to the three stages that divides a problem to be analyzed by the Finite Element Method (preprocessing, resolution and

post-processing) as explained in the section 5.2.1.

Actually ABAQUS is divided into four modules because in preprocessing the program distinguishes between explicit or dynamic analysis:

- ABAQUS-Standard, solves the traditional finite element analysis implicitly typed such as static analysis, dynamic low speed (both in time domain and frequency), thermal, etc, including contacts material and non-linearity. ABAQUS-Standard is integrated into ABAQUS / CAE for all the pre and post processing analysis.
- ABAQUS-Explicit, was introduced in 1991 as an explicit solver suitable for dynamic analysis at very high speed and quasi-static analysis, in which the non-linearities are evident, such as contacts, large deformations, etc. Examples of these applications are crash tests in automotive, free fall test, stamping and forging processes, etc. ABAQUS allows begin an analysis in ABAQUS / Standard and use the results as initials conditions of analysis in ABAQUS / Explicit, and vice versa.
- ABAQUS-CAE, is an effective tool and highly customizable to create finite element models in an interactive way, view test results and automating processes using scripts or subroutines in Python. With ABAQUS-CAE can be create the finite element model form geometry that is created in the same program or import it directly from common CAD formats, or also directly import another mesh finite element software, such as MSC.Nastran.
- ABAQUS-Viewer, is a visualization module of solutions. Shows the results obtained once solved the problem.
- ABAQUS-CFD, is a module that allows analysis of fluid dynamics or CFD (Computational Fluid Dynamics) integrated into the pre and post processor ABAQUS-CAE. Highlights the ability to perform coupled simulations interacting fluid and structure and simulate both structural and thermal conditions.

To solve a problem with ABAQUS it must be introduced an input data needed by the program. This step corresponds to the stage of preprocessing in Finite Element Method. The input data are introduced into the program through a text file(input file) that contains all the information needed to perform the simulation. This text file, also called *input file* can be created interactively using ABAQUS / CAE, internally generated the text file, or using a text editor, where the file is written directly by the user.

The data that are entered in the *input file* are of two types, *model data* and *history data*. The *data model* used to define the finite element model are divided into:

- Geometry. The geometry is the first thing that is introduced and must represent as accurately as possible the real body to be studied. ABAQUS allows very complex geometry models, through the module ABAQUS-CAE. The geometry and the mesh of a model is defined by the elements and nodes.

- Material. The model that is implemented can be formed of various materials. It is necessary to define the properties of different materials that our model is based on, and must be associated with parts of the geometry that apply.
- Parts and Assembly. The geometry model can be defined organizing it in parts, therefore, it must be entered in the input file relationships between these parts, in addition to the relative position of one part respect to each other.
- Initial Conditions. Must be specified the initial conditions of the model. Sometimes it is necessary to specify initial conditions different from zero for stresses, temperatures, speeds, etc.
- Boundary Conditions. The model may be subject to certain impositions by their environment that must be specified in the input file. It may be imposed restrictions on the movement, values displacements and rotations or symmetry conditions.
- Interactions. Occasionally the model that is studied can be formed by several bodies at a given time and suffer a contact or a interaction. ABAQUS also allows models to these situations.
- Amplitude Definition. Certain loading conditions and boundary conditions can be defined in terms of time, so you must enter the parameters of the curves that define these states of loads and boundary conditions.
- Environment Properties. You can define the characteristics of the environment, as may be the humidity, temperature, pressure, etc.
- Continued Analysis. It involves inserting results of preliminary analysis to continue searching results with the new model.

After loading the input file into the program, it is proceed to the resolution of the model. This stage is internal and on it ABAQUS does not interact with the user. Once ABAQUS solved the model, the simulation results are observed through the display module, which reads the output data file(output file), and is able to create animations of simulation, graphic, results tables, etc. Displaying results corresponding to the post-processing stage of the Finite Element Method.

5.3 FEM Frequency Test

This section describes the general model which is used to carry out the frequency sweep simulations. It is justified the geometry adopted in our simulations based on other tests that have been carried out by IVBT institute with which we want to make comparisons. A part from this, it is explained the biofilm behaviour based on a subroutine implemented in ABAQUS. Finally we describe the boundary conditions and interaction between parts of the simulation. It is justified the loads and its values used for these simulations.

5.3.1 Definition of Geometry

The simulations have been carried out are implemented according to the rheological tests that have been conducted at the IVBT institute. As explained in section 5.1 in the frequency test it has been used plate-plate geometry. It is discussed the geometric dimensions of both sample and plates.

Plates

The geometry that has been used was plate-plate. The upper plate was defined as a shell from a rigid body. Thus the only dimension to consider is the diameter of the plate.

The plates that have been used PP40 so the diameter of each plate must be 40mm. Having the same dimension as the sample plate convergence problems appeared. Because of this we have taken the upper plate diameter as 41mm to avoid this problem.

At the time to define the geometry of the plate we added a reference point for the entire plate. This reference point is used to get the values of torque, force, displacement and rotation of the plate. With these values we can calculate any variable of our study.

Biofilm Sample

The biofilm sample that has been tested must be a cylinder with diameter equal to the plates used in the rheometer. The reports indicated that this type of testing has been carried without a Petri dish. Thus the sample has the same diameter as the plate with which it is tested. We take as geometry a cylinder with diameter of 40mm.

We justify this choice also through the manuals about rheometry[3] and through Bohlin rheometer own manual[6]. It is explained that the sample should just fill the gap between the upper and lower elements. If too much or too little sample is used, the torque produce will be incorrect leading to the data being higher or lower respectively. The best results can often be obtained by pre-forming the sample into a disc of the same diameter of the upper plate.

Defined the diameter of the sample, it is now chosen which will be the height of this. This sample height called gap is one of the critical dimensions of the geometry. The reason for this narrow gap is to obtain a shear rate distribution across the gap which is effectively constant. The "gap loading limit" is the maximum gap that a sample can fill whilst still giving a uniform velocity distribution across the gap[6]. According to the manual Thermo Haake rheology[3] this distance should be not smaller than 0.3mm and not larger than 3mm since otherwise sizeable measuring errors related to the nature of the sample cannot be avoided.

In the test description of the IVBT institute it is indicated that the gap has been determined visually using a caliper and recorded manually. This institute has offered us the

range of values of the gap height used in their tests. The gap of the samples varies between 1.3-1.75mm. All measurements are in the range which indicates the rheometry manuals. Therefore in the simulations we set a gap height of 1.5mm.

Mesh

The mesh that has been selected to mesh the elements is a *Hex-dominated-Sweep-Medial axis* mesh. It has been taken this type of mesh because both geometries have radial symmetry. Thus it is reduced the number of nodes providing a lightest computation of the simulation avoiding lose precision. At the moment it is defined the type of meshing is also defined the type of integration. It is selected the type of *hybrid* integration since previously it is considered both the plate and the sample incompressible.

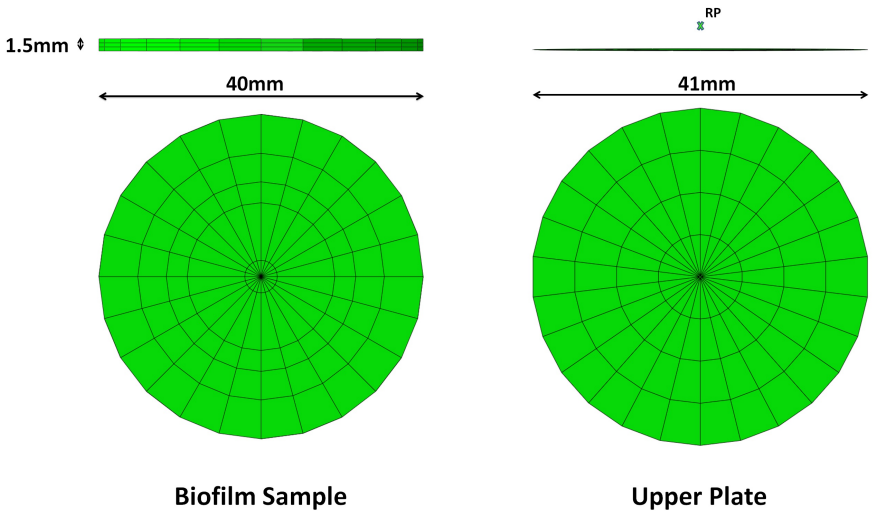

Figure 5.2: Representation of the two elements created for the frequency sweep. The biofilm sample is a deformable solid with cylindrical geometry. The diameter of the sample is 40mm and has a height of 1.5mm. The upper plate is a discrete shell with a circular geometry. The plate diameter is 41mm. It is defined a reference point(RP) for this discrete shell. Both geometries are meshed using a hexagonal dominated mesh and taking advantage of its radial symmetry.

5.3.2 Definition of Biofilm Behaviour

Before explaining how it has been implemented the viscoelastic behavior of the biofilm sample, we are going to comment how we defined the rheometer plate. It is considered the plate as a rigid body against the sample.

Rheometers plates are usually made with aluminum alloys which are incompressible and its deformation by biofilm tests do not change their geometry. Thus considered the plate as an undeformable rigid body, it is not necessary to define any material on this body. This way it is avoided defining the plate as a deformable body and with properties such as aluminum, simplifying the calculations when the computer is simulating.

Once explained how it is defined the rheometer plate it is explained how is defined the biofilm behavior. In section 3.3 is explained that the biofilm has a viscoelastic response to shear and normal stresses. Due to this is necessary to define the sample material as a viscoelastic material with their corresponding parameters.

ABAQUS gives the option to define a viscoelastic material through a frequency function or a function of reduced time. The time domain viscoelasticity is defined by a Prony series expansion. To implement this option is necessary that the step must be dynamic instead of static. This would be the common way to define a viscoelastic material. In this case the viscoelastic behavior is defined by a subroutine implemented in a static step.

The material law is implemented computationally as a user defined subroutine (UMAT). It can be used to define the mechanical constitutive behavior of a material; it must update the stresses and solution-dependent state variables to their values at the end of the increment for which it is called and it must provide the material Jacobian matrix, for the mechanical constitutive model; it can be used in conjunction with user subroutine USDFLD to redefine any field variables before they are passed in. The user should redefine only those variables identified as "variables to be defined".

The subroutine that has been used in these simulations has been implemented based on the work of Alexander E. Ehret [5] which proposes a mechanical model of microbial biofilms. The material law of this work have been previously described in section 3.3. This subroutine is implemented to define the behavior of biofilm based on n_i types of chains. Therefore it is possible to simulate the sample with different number of chains.

Each type of chain is defined by a number of parameters that the user inputs before the simulation. The order of these parameters such that relaxation times T_i increases. These parameters are:

- n_i : Number of chains per network in $10^{23}/\mathrm{m}^3$.
- L_i : Contour lenght in nm.
- lp_i : Persistence length in nm.
- T_i : Relaxation time in s.

Apart from defining these four variables for each chain, is necessary to define the value of another four variables. For all the simulations these variables will not be changed:

- ctemp : Temperature in K. The IVBT institute carried out the test at a temperature of 26 degrees celsius. Thus we define a temperature of 299 K.
- kappa : Compression modulus. It is given a high value of 100000000 to suppose incompressible the biofilm sample.
- runtim: The complete runtime of the job. In the instructions for use of the subroutine is indicated that if this value is unclear use a value of 10^6. Is taken this value as 10^6.
- rang: Integration domain. Is taken this value as 10.

For each simulation must be inputted four values for the parameters of each chain and the other four values which has been considered constant in our tests. These values are given below for each of the simulations.

5.3.3 Boundary Conditions

In a frequency sweep a constant stress or strain is applied(always in the linear region) and studied the response of the material in a range of frequencies. To simulate this test is necessary to define conditions for the sample fix and define the interaction between the sample and the plate. Defined this interaction it is proceed to define loads and times in the oscillation test.

Sample Interactions

The test is performed using plate-plate geometry. The sample is placed above the bottom plate and maintained in that position throughout the test. Therefore it is considered that the sample is embedded in its under side and it is used the *Encastre* option as boundary condition.

In order to define the contact between the upper plate and the sample at all times is defined condition of contact between both surfaces. Also is added a compression load to ensure this contact.

To set the interaction between the two surfaces gelling is assumed that the character of the sample allows full adhesion to the upper plate. Thus it is defined a *Surface-to-surface contact* between both surfaces. The tangential behavior is formulated as *Rough* so no slip will occur once points are in contact. The normal behavior is formulated as *Hard Contact* and is not allowed separation after contact.

The compression load is defined in one step previous to the simulation of the oscillation. This load is applied proportionally in 1 second, in one step of 5 seconds and is kept constant the rest of the test. According to the work of IVBT institute the rheometer applies a force of 2N on this compression. It is defined a displacement of the upper plate

with value of $3 \cdot 10^{-5}$mm and checked that the force applied ensures hard contact. It is assumed that this force does not influence the shear stresses applied in the frequency-sweep.

Oscillation Loads

As the rheometer has to work within the linear region[6], both tests and simulations has carried out with a shear strain of 1%. This deformation is relative to the height of the gap and must be inputted in ABAQUS as an angular rotation. Therefore,

$$\begin{aligned} H_0 &= 0.01 \cdot H_{sample} = 0.015[\text{mm}] \\ L_0 &= 2 \cdot \pi \cdot R_{sample} = 125.66[\text{mm}] \\ dH &= H_0/L_0 = 1.1936 \cdot 10^{-4} \\ UR3 &= dH \cdot 2 \cdot \pi = 0.00075[\text{rad}] \end{aligned}$$

where H_{sample} is the height of the gap, considered as 1.5mm, R_{sample} is the radius of the sample considered 20mm, and UR3 is the oscillation amplitude in radians carried out by the rheometer.

The frequency sweep that is performed in the simulation has a frequency range of 0.1-10 Hz. To simulate the spectrum of frequencies of 0.1 to 10 Hz there are defined certain oscillation steps for specific frequencies. It is defined eleven for these frequencies of oscillation: 0.1Hz; 0.2Hz; 0.4Hz; 0.6Hz; 0.8Hz; 1Hz; 2Hz; 4Hz; 6Hz; 8Hz; 10Hz. In each one of these steps there are defined the rotation amplitude, UR3, which is equal for all steps, and the angular frequency of each frequency as $\omega = 2\pi f$. With these values it is completely set the oscillation steps for each frequency.

In order to have a more accurately simulation of the test, the IVBT institute was asked about how the rheometer worked in the frequency sweep. The rheometer performed intermittently the oscillations while is increased the frequency value. It is assumed that the oscillations are carried out intermittently to allow the sample relax between different frequency oscillations.

Due to this it is defined one relaxation step between each oscillation, which does not apply any rotation, so that the sample begins the next oscillation completely relaxed. Taking these steps of 25 seconds the sample begins relaxed the following oscillation.

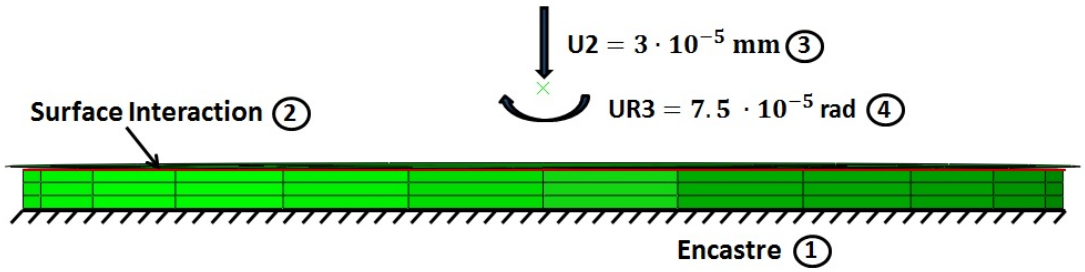

Figure 5.3: Boundary conditions applied in the frequency sweep: 1. Embedment of the biofilm sample on its lower face. 2. Contact interaction between the upper plate and the sample defined as adhesion. It is not allowed separation between both bodies. 3. Compressive load to ensure adhesion. Compression is applied until reaching the value of $3 \cdot 10^{-5}$ mm and ensures hard contact. This force does not affect the values of the frequency sweep. 4. Angular rotations for each frequency tested. It has rotation amplitude of $7.5 \cdot 10^{-5}$ mm and the rotational speed for each step is proportional to the corresponding frequency.

5.4 FEM Compression Test

This section describes the general model which is used to carry out the compression test simulations. In this particular case it is justified the geometry adopted in our simulations based on the compression experiments for characterization of biofilm behaviour at large strains, evaluated with Maple software by Alexander E. Ehret[5]. For these simulations is only employed the material that defines the behavior of biofilm. The last section describes the boundary conditions and the applied loads. These conditions and loads are justified from the calculations performed in the work of Alexander.

5.4.1 Definition of Geometry

The compression of biofilms evaluated in the previous work illustrate the compressive stress response for an homogeneous uniaxial compression. Therefore for these simulations is only necessary to define the geometry of the sample to be compressed.

Biofilm Sample

The biofilm sample that has been tested is a cube of unit sizes. Is generated as a 3D deformable solid. This is the simplest geometry that can be created to simplify calculations when it is performed the simulation. Therefore the geometry used here is a 1m x 1m x 1m cube.

Mesh

The mesh that has been selected to mesh the element is a *Hex-Structured* mesh. It has been taken this type of mesh because this is the simplest mesh that can be defined for a unit cube. Thus it is reduced the number of nodes providing a lightest computation of the simulation avoiding lose precision. As has also been made in the simulation for the frequency sweep, when is defined the mesh is also defined the type of integration. Again is selected the type of *hybrid* integration since previously it is considered both the plate and the sample incompressible.

5.4.2 Definition of Biofilm Behaviour

As already defined in section 5.3 which describes the frequency sweeps, the biofilm has a viscoelastic response to shear and compressive stresses. It is again necessary to define the sample material as a viscoelastic material with their corresponding parameters.

UMAT subroutine is again used to define the behavior of the material. Also is redefined for each simulation four values for the parameters of each chain and the other four values which has been considered constant in our tests.

5.4.3 Boundary Conditions

It is already mentioned that these test are homogeneous uniaxial compressions. It is therefore necessary define the boundary conditions that determine uniaxial compression. Below is explained these conditions and described how compression is applied to the body deformation.

Symmetric Conditions

These compression are carried out with lateral extension because this simple configuration serves well to highlight the basic characteristics of the model. As a consequence of this are setted symmetric conditions in the main planes that contain the cubes. In this way, it is selected the main planes and created the *XSYMM*, *YSYMM* and *ZSYMM* symmetries.

Compression Load

In the article of Ehret[5] it is assumed that the biofilm sample is compressed with a constant rate α_λ. The stretch $\lambda(t)$ is given as the ratio of current to initial height of the biofilm sample at time t. Thus strecht can be reformulated as

$$\lambda(t) = 1 - \alpha_\lambda t \tag{5.1}$$

The constant rate α_λ is varied over four orders of magnitude with the following values: 0.0001s^{-1}, 0.001s^{-1}, 0.01s^{-1} and 0.1s^{-1}. The strecht is illustrated from a ratio value of 0.5 to a ratio value of 1.

To implement this compression, it is set a displacement of 0.5m in the Y-axis. To impose constant the strain rate is selected an amplitude in the form of *Ramp*. By defining, for each constant rate α_λ, the overall time of the deformation $t = t_{\text{final}}$ and setting the maximum strecht value as $\lambda\left(t_{\text{final}}\right) = 0.5$ it is achieved this constant compression.

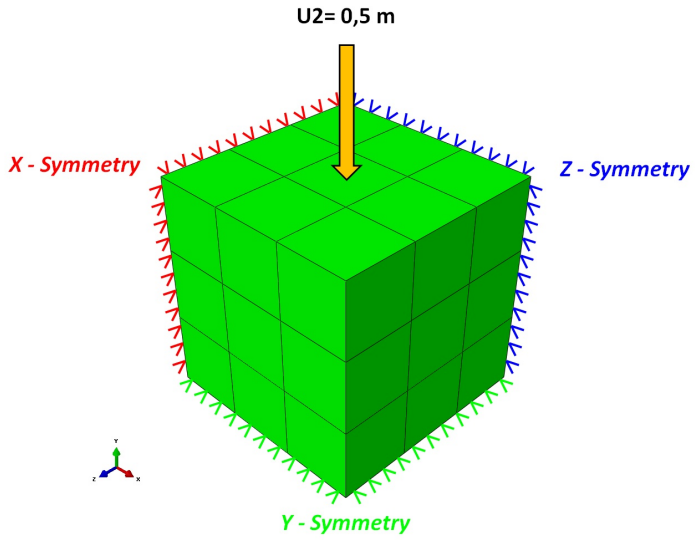

Figure 5.4: Boundary conditions applied in the compression tests. Biofilm sample is represented as a cube of unit sizes, 1m x 1m x 1m. As can be observed from picture the mesh used in simulations is *Hex-Structured*. To impose an homogeneous uniaxial compression is set the *XSYMM*, *YSYMM* and *ZSYMM* symmetries in the main planes. To perform the compression a displacement of 0.5m is applied in the Y-axis. The biofilm sample is compressed with a constant rate of strecht.

6 Results and Discussion

To investigate the mechanical properties of hydrogels, it is first checked the material behaviour at compression test to see how it works in the subroutine of the material at large strain. For this purpose, it is simulated compression tests at large strains which has been solved analytically on A.Ehret[5].

Once is studied the behaviour of the material at compression, it is checked if the model performed on the finite element program works in the same way that an oscillatory rheometer. Therefore it is simulated the frequency sweep shown in the above work and compared the outputs shown by the rheometer and the finite element model.

Lastly and once validated the frequency sweep model, the biofilm model parameters which define the behaviour of hydrogel with the influence of divalen cations such as Mg and Ca are obtanied. It is studied the influence by varying certain parameters, as are the number of chains per network or the relaxation times of these chains. These simulations are subtantiated on certain assumptions about the mechanical behaviour of Gellan. Finally it is compared the curves obtained by these simulations on finite elements against the rheological results obtained by Kaptsan[11].

6.1 Compression Tests at Large Strains of *P.aeruginosa*

Compression tests are the simplest way to perform the characterization of biofilm behaviour at large strains. As has already been mentioned it is simulated the compression test which has been solved analytically on A.Ehret[5]. This test is simulated because it is known both results and parameters with which is modeled the material behaviour. Thus it is possible to observe the response that provides the implemented subroutine for the material at large strains and compare with the analytical results.

In section 5.4 the simulated model is explained and justified according to the conditions tested in the article. It has previously been metioned that in the referenced article is solved the homogeneous uniaxial compression of biofilms with different amount of calcium at different rates. Therefore is necessary define the parameters fo the material for each concentration of Ca.

The estimation of the material parameters for the finite strain model is based on a few assumptions[7][5]. The time constants T_i can directly be identified from small strain rhe-

ological data. It is assumed that the persistence lenght l_p is independent of the Ca concentration and setted as $l_p = 15$nm according to a study by Vold[44]. The contour lenght L_i of alginate chains of type 1-3 is setted to 200nm for illustration purposes and the remaining contour lenght are obtained from the distance of nearest neighbours. The overall number of chains n_i, obtained by experimental findings, is in agreement with ellastically effective chains estimated in Wloka[7].

The parameters defined in this way and used throughout these simulations are given in table 6.1 and table 6.2. Table 6.1 shows the parameters used in the subroutine of the *P.aeruginosa* biofilm for a calcium concentration of 1mmoll^{-1} and table 6.2 shows the paramenters for a calcium concentration of 10mmoll^{-1}.

Table 6.1: Parameters which define the four types of chains of *P.aeruginosa* biofilm for a calcium concentration of 1mmoll^{-1}.

i	T_i (s)	n_i (10^{23}m^{-3})	L_i (nm)	l_p (nm)
1	0.060963	0.27999	200	15
2	1.1088	0.32017	200	15
3	16.009	0.18087	200	15
4	1925.4	0.017489	119.94	15

Table 6.2: Parameters which define the four types of chains of *P.aeruginosa* biofilm for a calcium concentration of 10mmoll^{-1}.

i	T_i (s)	n_i (10^{23}m^{-3})	L_i (nm)	l_p (nm)
1	0.060963	0.38795	200	15
2	1.1088	0.82435	200	15
3	16.009	0.79681	200	15
4	1925.4	1.9265	42.510	15

The results obtained in the ABAQUS simulations are illustrated in figure 6.1. It shows the nominal stress, P_c, versus stretch, λ, in the uniaxial compression with the different amount of calcium, 1mmoll^{-1} and 10mmoll^{-1}. It is illustrated the compressive response at different constant rate α_λ, which varies over four orders of magnitude from 0.0001s^{-1} to 0.1s^{-1}.

At first glance it is observed the influence of the concentration of calcium in the response of the material. With low calcium concentration, the material shows a throughout smoother response than with high concentration, where it shows a stiffer response. These results are in good agreement with the experimental results such as those given in Kaptsan[11]. The graph also reveals that for both employed concentrations the mate-

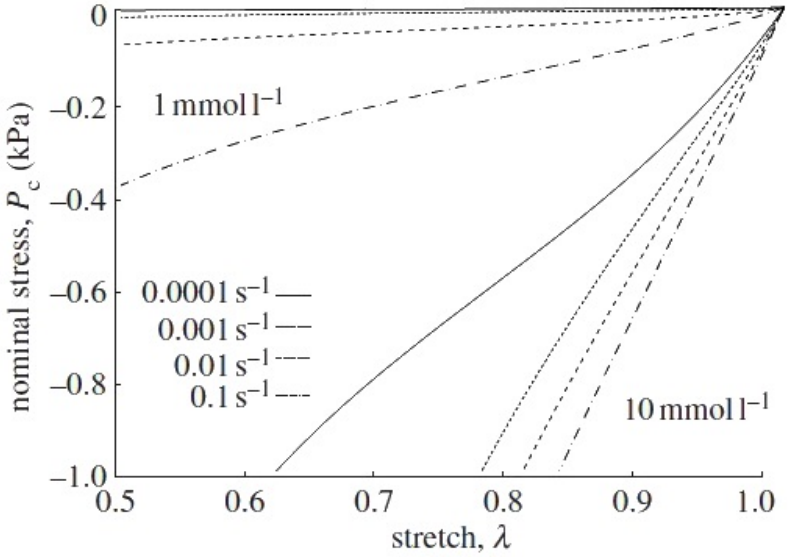

Figure 6.1: Simulated uniaxial compression using the subroutine implemented to biofilms. It is illustrated the nominal stressP_c versus stretch λ with two amounts of calcium, 1mmoll^{-1} and 10mmoll^{-1}. The sample is compressed with a constant rate α_λ which varies over four orders of magnitude from 0.0001s^{-1} to 0.1s^{-1}.

rial predicts stiffening with increasing strain rate. For the low calcium concentration the stress-stretch curves at rates of 0.0001s^{-1} and 0.001s^{-1} are nearly indistinguishable.

To check if the data obtained through the finite element program are admissible in figure 6.2 it is shown both graphs obtained in ABAQUS and the graphs obtained through analytical resolution by Ehret[5]. Comparing both graphs it can be observed that the behavior of the material is practically similar. For low concentrations of calcium the values generated by the subroutine are similar to those obtained through analytical resolution. In case of high concentrations of calcium the values obtained through finite element simulation differs from those calculated analytically. The response of the material through the subroutine in ABAQUS is less stiffer and is observed clearly in the response at rate of 0.0001s^{-1} for a calcium concentration of 10mmoll^{-1}.

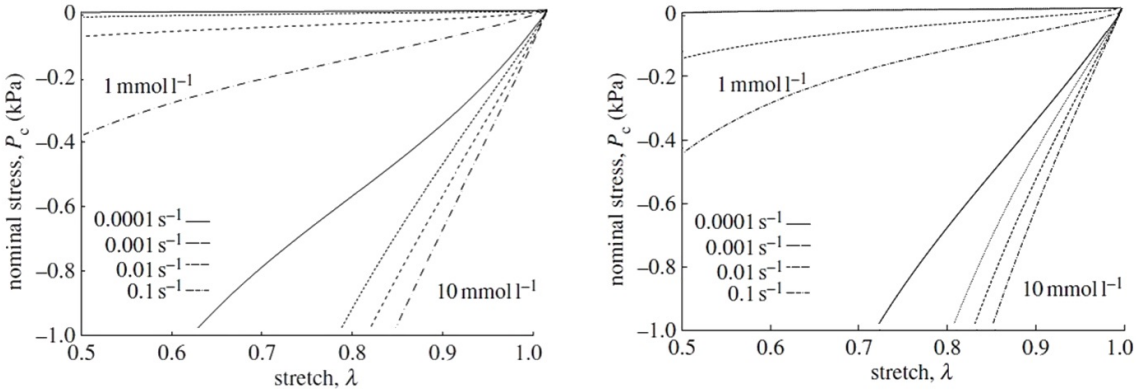

Figure 6.2: Figure a) shows the response of the material to an uniaxial compression test performed by ABAQUS software. Figure b) shows the response of the material to an uniaxial compression test solved numerically. It is illustrated the nominal stress P_c versus stretch λ with two amounts of calcium, 1mmoll^{-1} and 10mmoll^{-1}. The sample is compressed with a constant rate α_λ which varies over four orders of magnitude from 0.0001s^{-1} to 0.1s^{-1}.

6.2 Oscillatory Shear at Small Strains of *P.aeruginosa*

In this section, the finite element model simulated in ABAQUS is compared with experimental and analytical results given by Ehret[5]. The aim of validating this simulation, which models a frequency sweep, is to use this model in finite elements to estimate the parameters of biofilms or other viscoelastic materials through the data curves obtained in experimental test with a CS-rheometer.

It is again compared with this work for the reason that in this one it is estimated material parameters from rheological data. Thus it is possible to use these parameters in the finite element simulation and compare the results with those that can provide any laboratory CS-rheometer. Their study is based on Wloka[7], who tested *P.aeruginosa* with a parallel plate rheometer. Based on these tests and assuming a rheological model that consist of four parallel Maxwell elements, it is possible to estimate with equations 4.16 and 4.17 the time constants T_i of each chain.

The frequency sweep performed on tests by Wloka have a frequency range of 0.01 to 100 Hz. The simulated model in finite elements only works in a range of 0.1 to 10 Hz because the aim of this frequency sweep is to work with the data obtained by Kaptsan[11], so it is only used this part of the data. As well as the compression test of section 6.1 it is determined the four time constants referring to 1 or 10mmoll^{-1}. Therefore to assign the parameters to the material subroutine it is used the same parameters employed in the

compression tests. These values, for each calcium concentrations, are listed in table 6.1 and table 6.2.

The finite element model in ABAQUS with which it is recreated the frequency sweep is explained in section 5.3. Using model and based on the values of the parameters which are previously discussed it is possible to obtain for the frequency sweep the torque and delay at each instant of time. With these two values, which can be obtain from simulation, and applying the "form factors" cited by Bohlin[6] that are listed in equations 4.22 and 4.23, it is able to calculate the values for the elastic modulus G' and loss modulus G''. Should be remembered that these "form factors" are referenced to the $3/4$ radius position.

The results of simulations for both concentrations are presented in tables 8.1 and 8.2 in the annex. In them there are listed both simulation data and rheological values. The frequency sweep for each concentrations are illustrated in figure 6.3. It is shown the elastic modulus and loss modulus in a frequency range of 0.1 to 10 Hz.

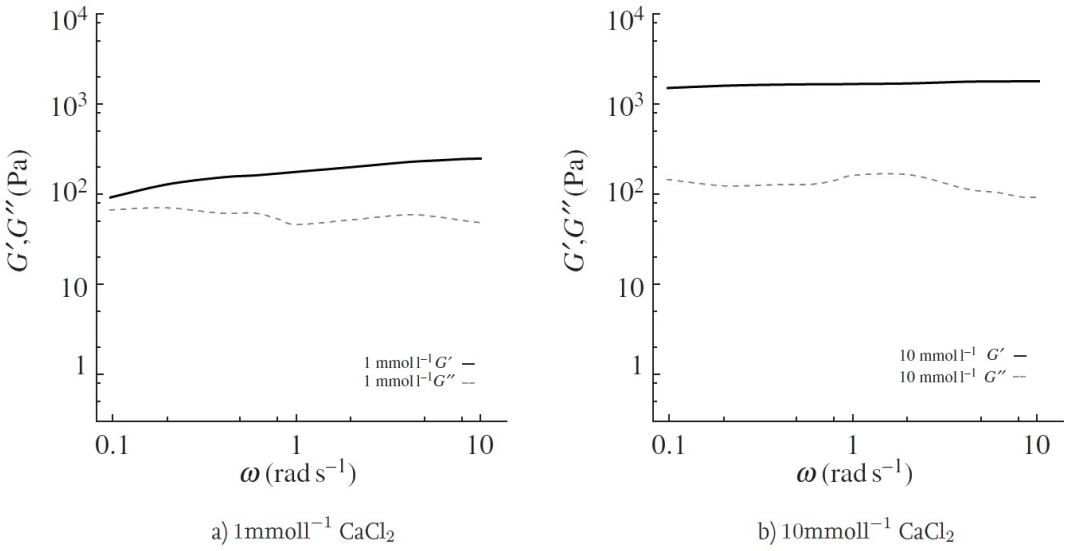

Figure 6.3: Frequency sweep performed in ABAQUS for *P.aeruginosa* with calcium concentration of a) 1mmoll^{-1} and b) 10mmoll^{-1}. It is illustrated the elastic and loss modulus curves at a frequency range of 0.1 to 10 Hz.

The curves obtained with ABAQUS simulations look in accordance with the results achieved in the compression test. For high calcium concentrations the value for the elastic modulus is between 1500-1800 Pa. In contrast, for low calcium concentrations the value for the elastic modulus is between 90-250 Pa. This difference is consistent with the tendency observed in the compression test where high concentrations shows a stiffer re-

sponse. The graphs also reveals that for low concentrations the phase angle, or delay, is between 11° to 36° which indicates ambivalent viscoelastic behaviour. However for high concentration this phase angle is between 3° to 6°. This value indicates elastic behaviour which is in consonance with the values obtained by Kaptsan[11].

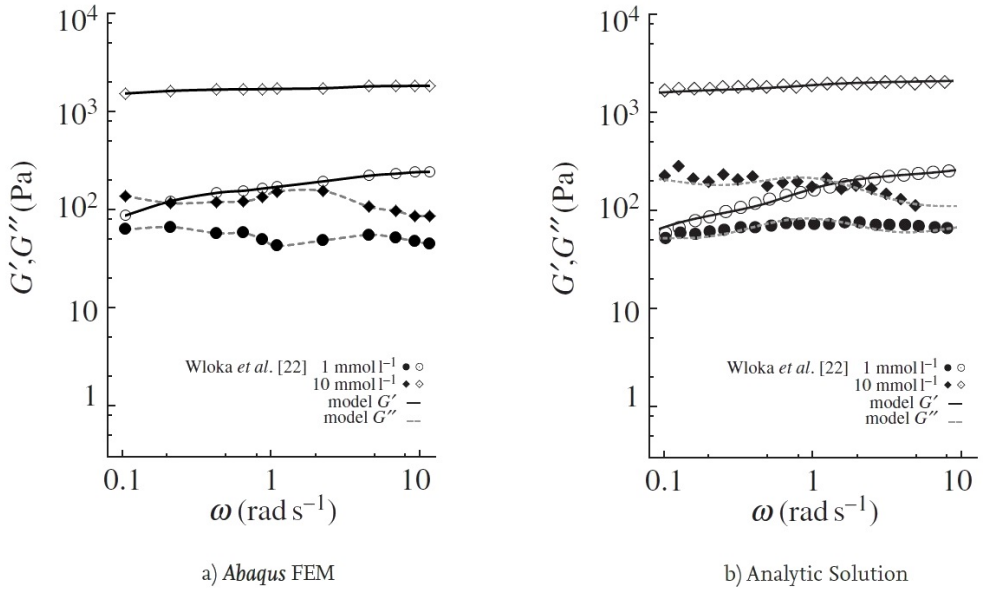

Figure 6.4: Comparison between the results of the frequency sweep in finite element and numerical calculation. Graph a) illustrates the elastic and loss modulus curves from the ABAQUS simulation. Graph b) illustrates the elastic and loss modulus from numerical calculation by Ehret[5] and experimental data by Wloka[7].

To get a clearer approach, figure 6.4 illustrates both graphs, where the results of simulations and those calcullated numerically by Ehret[5] are compared. The elastic modulus curves have the same values in both cases, appreciating in low concentration values slightly higher in the simulation than in the numeric calculation. In case of loss modulus curves is a different matter because their tendency is slightly different. This deviation may be due to two causes. The first is related to the definition of the simulated model. At some frequencies the delay is less than the increase time taken in the oscillation and it is not possible an accurtely determination of the delay. Thus the distribution between elastic and loss modulus may be wrongly distributed. The second reason is related to the "form factors". It is already mentioned that is necessary use these "form factors" explained in section 4.4 to get the elastic and loss modulus. This conversion may not fit with real values for the reason that the calculations are taken for a certain radius rather than take the shear stress for each length of the radius.

Despite these diferences it is assumed that the simulation which models the frequency sweep is valid to obtain values which can provide any rheometer. Therefore this model is used on the rest of simulations to get the parameters of the studied material.

6.3 Oscillatory Shear at Small Strains of Hydrogel

Once the frequency sweep model is prepared in ABAQUS software, the parameters to characterize hydrogels are obtained based on the experimental data by Kaptsan[11]. The hydrogel to be characterized is Gellan gum because it is the one that is used in these experiments. It is already mentioned that this hydrogel has been used because the EPS matrix shows similar viscoelastic properties as Gellan. They have developed the rheological characterization and have established the viscoelastic Gellan as a biofilm model.

Gellan gum is an exocellular anionic heteropolysaccharide produced by aerobic fermentation of the bacterium *Sphingomonas elodea* (formely kown as *Pseudomonas elodea*)[45]. The characteristic feature of Gellan gum is that it can produce thermoreversible transparents gels in aqueous solution, which depends on the kind and concentration of metallic ions. Gellan forms gells in the presence of mono and divalent cations. However, its affinity for divalent cations such as Ca and Mg is much stronger than monovalents such as Na and K. This difference in efficiency has been attributed to the difference in their gel-inducing mechanisms[46]. Rheological measurements also suggest that the elastic modulus of gels was increased by inmmersion of gels in water and in salt solutions, which can be attributed as the stiffening of network chains due to gel swelling, leading to an increase in elastic modulus with time[47] [48].

The conditions in this experiment are identical to the frequency sweep performed in section 6.2 with *P.aeruginosa* biofilm. The design of simulations is defined in section 5.3. In order to study the parameters of Gellan by influence of two divalent cations, it is required gellan solutions with $MgSO_4$ and $CaCl_2$. Therefore, the simulations are based on Gellan test for the following concentrations[11]: a) Gellan with $MgSO_4$: 0.5% Gellan, 0.03 M NaCl, 0.0084 M $MgSO_4$; b) Gellan with $CaCl_2$: 0.5% Gellan, 0.03 M NaCl, 0.0084 M $CaCl_4$.

To parameterize the Gellan from the biofilm model developed by Ehret[5], it is necessary to establish the values of four parameters (number of chains per network ,n_i, contour length ,L_i, persistence length ,l_p, and relaxation time ,T_i) for each type of chain. If Gellan is characterized with four types of chains it have to be fixed sixteen values. For this reason, certain assumptions are made to reduce the number of parameters to be obtained through out the simulations. To start with, values for relaxation time, contour length and persistence lenght are kept constant in the simulations and is only varied the number of chains per network to reach the experimental values.

Values for contour length ,L_i, and persistence length ,l_p, are chosen from the characterization of Gellan gum performed by Takahashi[49][50]. They achieve this characterization by using static and dynamic light scattering techniques focusing on the molecular-weight distribution. It is modelled the Gellan gum by the wormlike chain(WLC) model to reproduce the chain stiffness changes. The persistence lenght, l_p, the most important parameter characterizing the chain stiffness, was estimated as 98 nm at $25°$C. The contour length, L_i, was calculated and evaluated as 354 nm at $25°$C. These two values are set to the remaining simulations.

The relaxation times are estimated from the frequency sweep obtained by experimental test in the IBVT laboratories. As can be seen in figure 6.5 the frequency range is carried out at range of 0.1 to 10 Hz. Therefore it is only taken the values of the three faster relaxation times from both cation concentrations. The relaxation time of the slower chain is set again from the data obtained by Ehret[5].

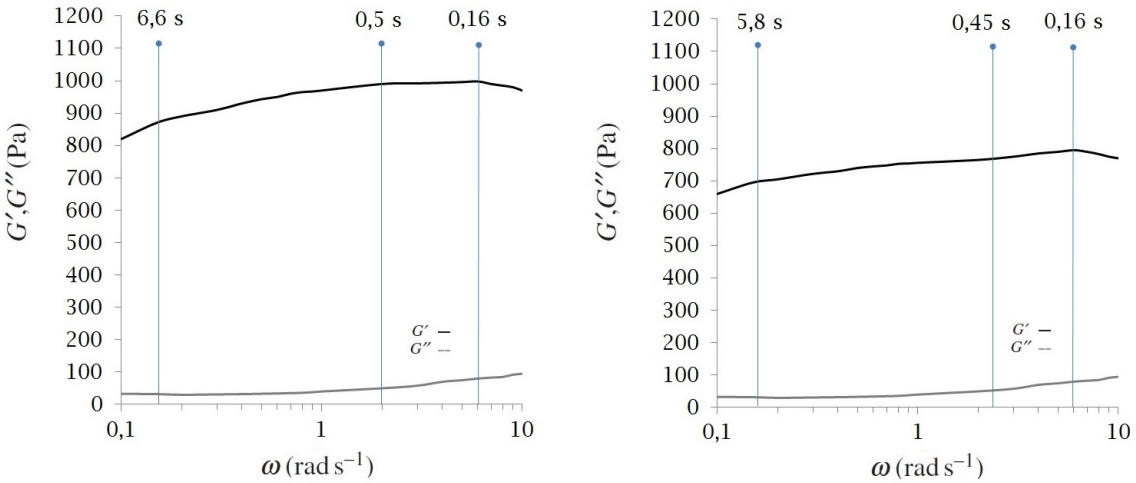

a) Hydrogel with Ca cations

b) Hydrogel with Mg cations

Figure 6.5: Experimental frequency sweep performed by Kaptsan[11] for gellan solutions with $MgSO_4$ and $CaCl_2$. Based on these curves the relaxation times of the three faster chains are estimated. These values are used in ABAQUS subroutine.

Fixing the values that are estimated as constants in simulations, the frequency sweeps of gellan solution with $CaCl_2$ are simulated taking as approximation for the values of number of chains per network the values of the previously tests with *P.aeruginosa* for both concentrations of Ca. Once several simulations have been carried out, it is established the frequency sweep curve for frequencies above 1 Hz. Therefore it is decided to set the parameters of the faster chains and just vary the number of chains per network of the

slower chain to see their influence on the curves. It is simulated the frequecy sweep with these values from the number of chains per network of the slower chain: 0.01; 0.8; 1; 1.93 $\left(10^{23}\mathrm{m}^{-3}\right)$. The values taken as constants are listed in table 6.3 for each of the chains.

Table 6.3: Values taken as constans from the model parameters to see the influence of the number of chains per network from the slower chain. The value of n_4 $(*)$, is varied by taking the following values: 0.01; 0.8; 1; 1.93.

i	T_i (s)	L_i (nm)	l_p (nm)	n_i $\left(10^{23}\mathrm{m}^{-3}\right)$
1	0.166	354	98	0.31036
2	0.5	354	98	0.65948
3	6.666	354	98	0.79681
4	1925.4	354	98	$*$

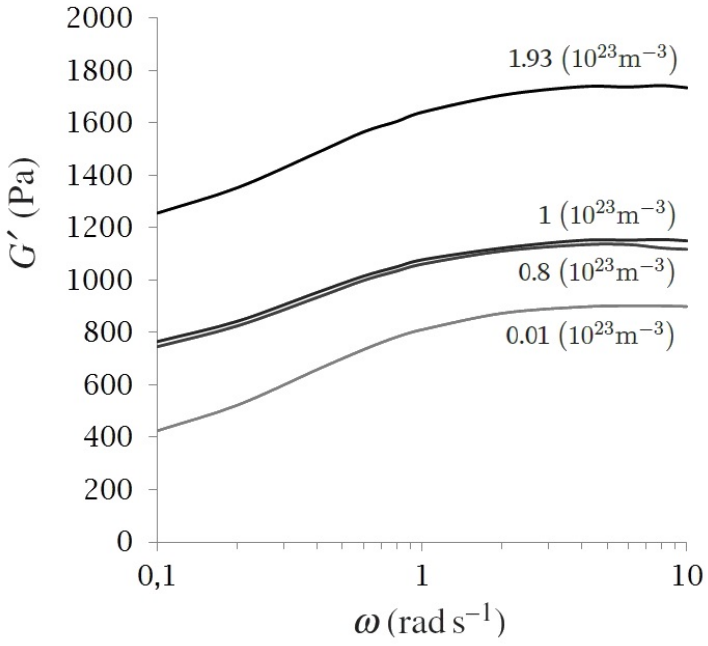

Figure 6.6: Influence of the number of chains per network n_4 by taking the rest of the parameters listed in table 6.3. Increasing the number of chains n_4 it is achieved only a stiffer behaviour of the gel, without changing its frequency dependence in this range.

Figure 6.6 illustrates only the curves of elastic(storage) modulus, G', for different values

of n_4. The loss modulus, value which does not exceed 100 Pa, is not represented because its value is nine times less than the elastic modulus. The elastic behaviour of the material is justified by the data of the simulations which shows a delay of $3.6°$. Also, its value in this frequency range does not vary respect n_4. These results justify the strong elastic character of Gellan gum. Besides this, according to the graph it is observed that variation in the number of chains n_4(slower chain) influences only on the modulus of the elastic component of the gel. Increasing the number of chains per reference volume is been getting a rigid gel so its elastic modulus increases. In contrast, it is also observed that the variation of the value n_4 does not influence the elastic modulus as a function of frequency for the frequency range which has been simulated. All curves have the same curvature against frequency even they have different number of chains.

For this reason and to achieve flatter curves that accord with the curves obtained in the rheometer by Kaptsan[11], see figure 6.5, the influence of the relaxation times of the two slower chains, in this case T_4 and T_3, is studied. Both, the values of chain lengths and the relaxation times of the first two chains are taken as the same way as the above simulations. The number of chains per reference volume of the slowest chain is taken as $0.7\ (10^{23}\mathrm{m}^{-3})$ based on the graph of image 6.6. Relaxation time T_4 is simulated for input values of 2500s, 1925s and 1000s. For the relaxation time T_3 are taken the values of 30s, 10s and 6.6s.

The curves obtanied for these simulations, which are illustrated in figure 8.1(annex), shown no change for any variation of these relaxation times. These results may be possible if the relaxation time of this chains has no influence on the frequency range from 0.1 Hz to 10 Hz. According to the fact that varying only the slower chains is not possible to obtain the response as a function of the frequency that is desired, is determined to move the relaxation times of the first three chains to higher values and see if they influece the elastic behaviour at low frequencies.

For this purpose is remained again values for contour length ,L_i, and persistence length ,l_p. The relaxation times are established with new values,increasing now the relaxation times of the first three chains with values of 0.5s, 10s and 100s respectively. In order to get a general idea of in which range works this new values it is set again the number of chains per network of the first three chains and varied the value of n_4 by taking the following values: 0.7; 0.6 and 0.4 $(10^{23}\mathrm{m}^{-3})$. All of these values established for the new simulations are listed in table 6.4.

The graphs resulting from these simulations are shown in figure 6.7. Once again, it is represented only the elastic modulus, G', for the same reason as in the previous simulation, its value is nine times less than the elastic modulus and does not vary respect this frequency range. With these new relaxation times it is seen from the graphs that the curves get flatter shape, approaching the experimental curves shape. Apart from this, it is again confirmed varying the number of chains per network of the slower chain, n_4, only influences the material stiffness increasing or decreasing it, but does not change their behaviour regarding the frequency in this range.

Table 6.4: Values taken as constans from the model parameters to see the influence of the new relaxation times. The value of n_4, $(*)$, is varied by taking the following values: 0.7; 0.6; 0.4.

i	T_i (s)	L_i (nm)	l_p (nm)	n_i $(10^{23}m^{-3})$
1	0.5	354	98	0.31036
2	10	354	98	0.65948
3	100	354	98	0.79681
4	1925.4	354	98	$*$

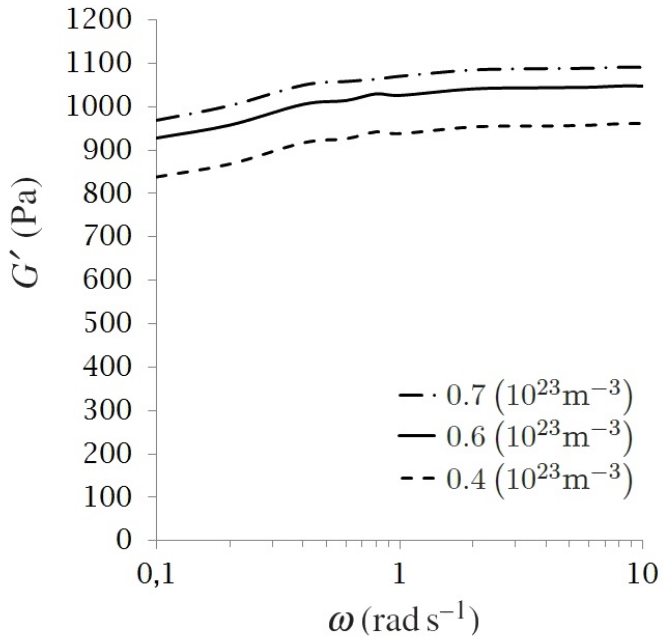

Figure 6.7: Influence of the number of chains per network n_4 by taking the rest of the parameters listed in table 6.4. With the new values of the relaxation times, for the elastic modulus, G', it is obtanied flatter curves.

For all these reasons and for the results that are already achieved, the following considerations are taken in order to obtain the parameters that lead to the graphs for both concentration of cations in the gellan. The number of chains per network of the slower chain, n_4, is the parameter that is used to get the necessary height of the curve, i.e. with this pa-

rameter it is controlled the value of the elastic modulus for the entire evaluated frequency sweep. The remaining number of chains per network is maintained with the values used heretofore. Furthermore values for contour length ,L_i, and persistence length,l_p are also kept the values used until now. Finally the relaxation time of the third chain, T_3, is set with different values trying to reach more or less flat curves and determine both values of this parameter to achieve the experimentally graphs reached by Kaptsan[11] for both concentrations of cations.

In order to study the influence of the relaxation time of the third chain, T_3, this parameter is evaluated for certain time values: 100s; 500s and 1000s. The remaining parameters have the values previously commented and are listed in table 6.5. With these simulations it is sought to obtain two different responses as a function of the frequency to determine the parameters of both Gellan with Ca cations and Gellan with Mg cations. The response of Gellan with Mg cations is flatter than the response of Gellan with Ca cations.

Table 6.5: Values taken as constans from the model parameters to see the influence of the relaxation time of the third chain, T_3. The value of T_3, $(*)$, is varied by taking the following values: 100s; 500s; 1000s.

i	T_i (s)	L_i (nm)	l_p (nm)	n_i $(10^{23}m^{-3})$
1	0.5	354	98	0.31036
2	10	354	98	0.65948
3	$*$	354	98	0.79681
4	1925.4	354	98	0.4

The curves of these simulations are shown in figure 6.8. In this case the curves are represented in a closed range of elastic modulus, G', to distinguish the variation from frequency. Based on the graphs, increasing the relaxation time of the third chain, T_3, the elastic modulus decreases at low frequences. The same effect appears for frequencies above 5 Hz where the elastic modulus also decreases. Therefore, and taking into consideration the curve shape of the experimental results in figure 6.5, it is chosen the relaxation time T_3 as 1000s for the behavior of Gellan influenced by calcium cations and taken the relaxation time T_3 as 100s for the behaviour of Gellan influenced by magnesium cations.

Based on these new relaxation times it is now possible to determine the parameters which define the rheologic response of Gellan influenced by calcium cations. In the case of the response of Gellan influenced by Mg cations is still necessary to get a response less stiff. Thus, one solution is to reduce the number of chains per network of the slowest chain n_4. For this purpose and with a relaxation time T_3 as 100s, it is simulated the frequency sweep taking the following values of n_4: 0.09; 0.08 and $0.07(10^{23}m^{-3})$. With these results it is possible to define the value of this parameter and have a response close to the experimental results.

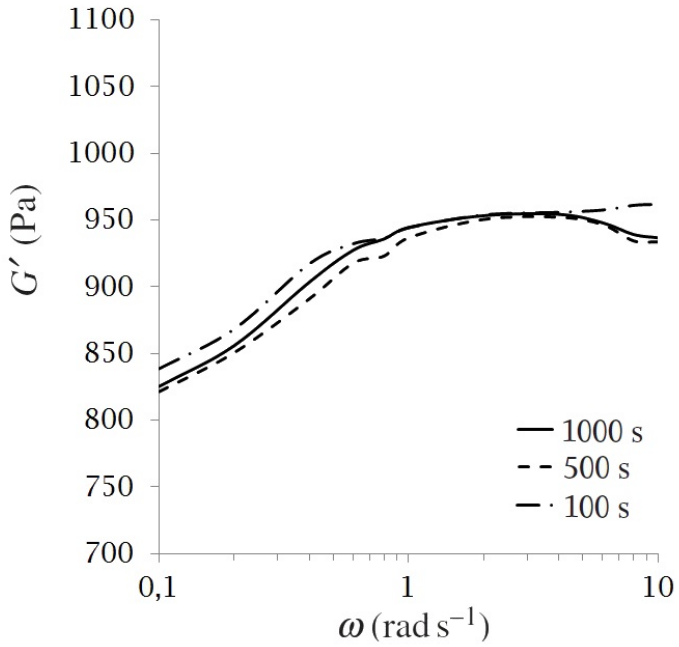

Figure 6.8: Influence of the number of the relaxation time of the third chain, T_3 by taking the rest of the parameters listed in table 6.5. Increasing the relaxation time T_3, the elastic modulus decreases at low frequences and for frequencies above 5 Hz.

The results of the simulations for a relaxation time T_3 as 100s are illustrated in figure 8.2 of annex. In them it is found that only varying the number of chains n_4 it is not possible to define the behaviour of Gellan with Mg cations. Again it is shown that decreasing the number of the chains per network of the slower chain only reduces the stiffness and there is no variation as a function of the frequency in this range. The best value that fits the curves obtained by Kaptsan[11] for Gellan with Mg cations is $0.07\left(10^{23}\mathrm{m}^{-3}\right)$. This value is chosen to define finally the desire response.

In tables 6.6 and 6.7 the parameters that have been taken as optimal to define the response of Gellan with both divalent cations are listed. Comparisons of the results obtained experimentally by Kaptsan[11] against the ones obtained from the finite element simulations in ABAQUS are illustrated in figures 6.9 and 6.10:

Table 6.6: Parameters selected to define the rheological behaviour of Gellan by influence of Ca cations.

i	T_i (s)	L_i (nm)	l_p (nm)	n_i $(10^{23}m^{-3})$
1	0.5	354	98	0.31036
2	10	354	98	0.65948
3	1000	354	98	0.79681
4	1925.4	354	98	0.45

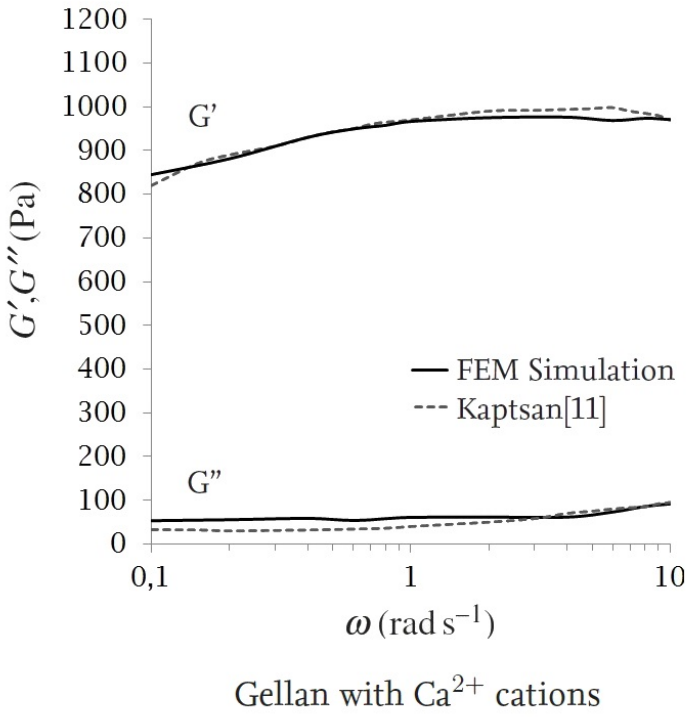

Figure 6.9: Curves of the storage modulus G'(Pa) and loss modulus G"(Pa) obtained in ABAQUS by using the values of table 6.6 for the parameters of the subroutine that modeled the biofilm behaviour by Ehret[5]. It also is shown the curves obtained by Kaptsan[11] through rheological tests on Gellan influenced by calcium cations. Can be seen that these parameters fit well the model implemented in ABAQUS subroutine to the experimental data.

Table 6.7: Parameters selected to define the rheological behaviour of Gellan by influence of Mg cations.

i	T_i (s)	L_i (nm)	l_p (nm)	n_i $(10^{23} m^{-3})$
1	0.5	354	98	0.31036
2	10	354	98	0.65948
3	100	354	98	0.79681
4	1925.4	354	98	0.07

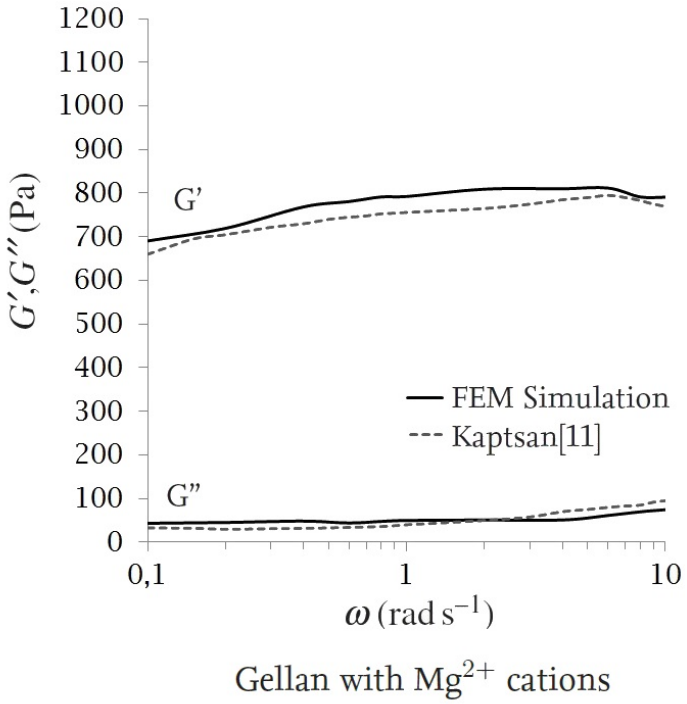

Figure 6.10: Curves of the storage modulus G'(Pa) and loss modulus G"(Pa) obtained in ABAQUS by using the values of table 6.7 for the parameters of the subroutine that modeled the biofilm behaviour by Ehret[5]. It also is shown the curves obtained by Kaptsan[11] through rheological tests on Gellan influenced by magnesium cations. Can be seen again that these parameters fit well the model implemented in ABAQUS subroutine to the experimental data.

Figures 6.9 and 6.10 demonstrate that the adjustment which has been performed with the parameters that define the biofilm model is close to the experimental results. The

response of the Gellan with calcium cations fits better to experimental values obtanied by Kaptsan[11] than the response of the Gellan with magnesium cations. That is due to the certain assumptions which have been made to set the values of certain parameters and be able to work only with a limited number of parameters. Otherwise the study of the behaviour of gellan based on sixteen parameters would be practically unfeasible. To improve the results it would be necessary to vary all the relaxation times and observe their influece regard to other variations. Apart from this, the breakdown of the complex modulus, G^*, in the storage modulus, G', and the loss modulus, G", may be due to the accuracy in simulations times. For certain frequencies the delay that is produced between stress and deformation is less than the increase time taken to this frequency sweep. Thus it is necessary to estimate the delay with a certain error.

Finally table 6.8 sets out the percent deviations of each point of the curves regarding to its experimental point. This is the only way to measure the deviation having only a sample of each data, data that are also a function of the frequency. The deviations are calculated in percentages of storage modulus, G', loss modulus, G" and complex modulus, G^*:

$$\text{Deviation}\,(\%) = \frac{\left|G_{\text{simulated}} - G_{\text{experimental}}\right|}{G_{\text{experimental}}} \cdot 100 \tag{6.1}$$

Looking at the deviation of the loss modulus, it seems that the error is considerable. This is due to the comparison is made between values of identical curves regardless of the difference in scale between the storage modulus, G' and the loss modulus, G". For this reason the measure which gives us a realistic insight of the deviation in our results is the deviation of the complex modulus, G^*, defined as a combination of the above modulus, see equation 4.12. The deviation of the complex modulus, G^*, for the simulated model of Gellan with calcium cations is not higher than 4% and for the model of Gellan with magnesium cations is not higher than 6%. Based on the table it is seen that deviations are reduced so the model approximates quite well to the experimental results.

Table 6.8: Percent deviations between the simulated and experimental values for Gellan with calcium cations and Gellan with magnesium cations.

Frequency(Hz)	G'$_{Ca^{2+}}$(%)	G"$_{Ca^{2+}}$(%)	G*$_{Ca^{2+}}$(%)	G'$_{Mg^{2+}}$(%)	G"$_{Mg^{2+}}$(%)	G*$_{Mg^{2+}}$(%)
0.1	3.03	61.06	3.15	4.65	31.68	4.72
0.2	1.00	84.79	0.86	2.05	50.88	2.16
0.4	0.01	82.83	0.13	5.30	51.12	5.40
0.6	0.08	58.05	0.02	4.81	30.01	4.87
0.8	0.76	60.65	0.65	3.67	30.96	3.74
1	0.38	51.99	0.26	4.84	24.66	4.90
2	1.51	22.69	1.44	5.79	1.84	5.78
4	1.79	12.26	1.84	3.22	27.17	3.02
6	2.95	8.54	2.98	2.13	23.33	1.90
8	1.15	1.03	1.13	1.07	17.89	0.86
10	0.07	3.42	0.04	2.71	21.30	2.39

7 Conclusion

In this work the rheological properties of hydrogels was examined, particularly it was characterized the behaviour of Gellan influenced by divalent cations such as calcium and magnesium. This characterization was performed through an inverse finite element approach via ABAQUS software.

The aim of this work was to get through finite element the parameters which define the subroutine implemented by Ehret[5] to be able to simulate the behaviour of hydrogels. To this end and in order to join experimental results with numerical results, this characterizaration was based on laboratory work done by Kaptsan[11]. In that work a series of experiments were conducted to determine the viscoelastic behaviour of hydrogels on Gellan base and also the influence of the divalent cations on the gel strength was studied.

For this purpose, a frequency sweep was modelled in ABAQUS to perform the oscillation test in the simulations. The design of this frequency sweep was based on how the CS-Bohlin rheometer is operated, this is the one used in these experiments. The rheometer was designed with a plate-plate geometry as it is the one used in the test. At this point a mention should be made to the desing of other geometries, that can be used with a rheometer for the same oscillation test, which could assist us in studying the collected data and be able to validated them.

Continuing with the details about the design of the simulations, it is necessary to discuss how the rheological values that have been obtained for the results were calculated. It have been used the form factors which suggest the manuals of CS-Bohlin rheometer to convert the torque and strain to the rheological values. This conversion is based on a simplification of the torque measured to $3/4$ of the maximum plate radius. As an alternative, it could be obtained a better approximation if it the applied torque were calculated as a function of the plate radius.

Last thing to be mentioned about the design of the frequency sweep is the interval of time used in the measurements. In the last simulations about the characterization of Gellan it has been seen that the delay between stress and deformation was below the interval of time that was taken to obtain those values. Due to that the distribution between the storage modulus, G', and the loss modulus, G", may differ from the real values. In order to refine the value of the delay it would be necessary to decrease the interval of time between each measurement. On the other hand, this step would lengthen the duration of the simulation, time that for this interval is already too long.

Having designed the frequency sweep in ABAQUS and before carrying out the rheological characterization, the compression tests of *P.aeruginosa* sample calculated numerically by Ehret were performed. From these simulations it was expected to evaluate the behaviour of the subroutine implemented by Ehret and compare it with the numerical results. The values obtained in the simulated tests were consistent with those obtained by numerical resolution. It is also true that the results of the simulations show a stiffer response for both, high and low, concentration of calcium. This could be due to numerical values were calculated for a single material unit and in ABAQUS software the simulations were performed for a full geometry.

After examining the compression behaviour provided by the subroutine from parameters already calculated, it was simulated the frequecy sweep again calculated numerically by Ehret for a sample of *P.aeruginosa*. Based on the parameters provided by the study of Ehret, the frequency sweep was performed for both calcium concentrations which had been tested by means of a rheometer by Wloka[7]. The curves obtained by simulations for both concentrations of calcium were fitted relatively to the experimental curves. This provides the thought that the designed model in ABAQUS validly performs the frequency sweep for that frequency range. Once again the curves show a certain stiffness against data obtained numerically, which is consistent with the results of compression tests.

Finally it was simulated the response of Gellan influenced by divalent cations such as calcium and magnesium in the designed frequency sweep. To be able to parameterize the hydrogel by the biofilm model is necessary to determine the value of sixteen parameters. That is the nub of the problem with this characterization, it is very complicated to determine validly each one of the parameters based only in rheological tests. Is necessary to take additional information with which it can be predetermined the values of certain parameters. In this case, the values of the characteristic lenghts of the chains were set from supplementary investigations on Gellan. From here it was studied the influence of the variation for certain parameters such as the relaxation time and the number of chains per network. Even thougth this simplification it was very complicated to control the response of the hydrogel because it was not independent parameters and its variation also affect the response for the other parameters.

The responses finally obtained through simulations were fitted to the measurements as a function of the frequency obtained in testing on rheometer for both Gellan with calcium cations and Gellan with magnesium cations. In the first case the deviation of the measurements is less than 4% and for the second case the deviation is less than 6%. With these results it can be concluded that the parameterization which has been performed about the Gellan is truthful to the experimental results obtained by Kaptsan. This does not mean that the obtained parameters are those who actually characterize the hydrogel because it is possible that from other parameter combination it can be reach the same answer. For this reason it is emphasized the need to resort to complementary studies in order to carry out these characterizations based on the biofilm model implemented in ABAQUS and applied in this frequecy sweep.

8 Annex

Oscillatory Shear at Small Strains of *P.aeruginosa*

Table 8.1: Values obtained in the frequency sweep simulated with ABAQUS for a *P.aeruginosa* sample with calcium concentration of 1mmoll^{-1}.

ω (Hz)	Torque (10^{-5}Nm)	Shear Stress (Pa)	Shear Strain	Shear Modullus (Pa)	Delay (s)	Delay (rad)	G' (Pa)	G" (Pa)
0.1	1.875	1.119	0.01	111.915	1	0.628	90.541	65.782
0.2	2.418	1.443	0.01	144.353	0.4	0.502	126.498	69.542
0.4	2.748	1.640	0.01	164.021	0.15	0.376	152.503	60.380
0.6	2.871	1.713	0.01	171.353	0.096	0.362	160.253	60.669
0.8	2.956	1.764	0.01	176.454	0.06	0.301	168.490	52.414
1	3.036	1.812	0.01	181.214	0.04	0.251	175.521	45.066
2	3.436	2.051	0.01	205.118	0.02	0.251	198.674	51.010
4	3.915	2.336	0.01	233.678	0.01	0.251	226.336	58.113
6	4.075	2.432	0.01	243.225	0.006	0.226	237.058	54.555
8	4.192	2.502	0.01	250.227	0.004	0.201	245.186	49.972
10	4.225	2.521	0.01	252.174	0.003	0.188	247.707	47.252

Table 8.2: Values obtained in the frequency sweep simulated with ABAQUS for a *P.aeruginosa* sample with calcium concentration of 10mmoll^{-1}.

ω (Hz)	Torque (10^{-4}Nm)	Shear Stress (Pa)	Shear Strain	Shear Modullus (Pa)	Delay (s)	Delay (rad)	G' (Pa)	G" (Pa)
0.1	2.526	15.077	0.01	1507.781	0.15	0.094	1501.089	141.894
0.2	2.677	15.977	0.01	1597.718	0.06	0.075	1593.178	120.350
0.4	2.755	16.445	0.01	1644.563	0.03	0.075	1653.965	124.942
0.6	2.779	16.586	0.01	1658.678	0.02	0.075	1656.963	138.579
0.8	2.786	16.627	0.01	1662.748	0.016	0.083	1656.963	138.579
1	2.805	16.740	0.01	1674.070	0.015	0.094	1666.64	157.543
2	2.848	16.999	0.01	1699.937	0.0075	0.094	1692.393	159.978
4	2.968	17.711	0.01	1771.151	0.0025	0.062	1767.656	111.211
6	2.985	17.812	0.01	1781.243	0.0015	0.056	1778.396	100.673
8	3.000	17.905	0.01	1790.560	0.001	0.050	1788.298	89.965
10	2.995	17.875	0.01	1787.534	0.0008	0.050	1785.276	89.813

Oscillatory Shear at Small Strains of Gellan

Table 8.3: Values obtained in the frequency sweep illustrated in figure 6.6 . The parameters used are listed in table 6.3 . The value of n_4 is set as 1.93 $\left(10^{23}\mathrm{m}^{-3}\right)$.

ω (Hz)	Torque (10^{-4}Nm)	Shear Stress (Pa)	Shear Strain	Shear Modullus (Pa)	Delay (s)	Delay (rad)	G' (Pa)	G" (Pa)
0.1	2.109	12.588	0.01	1258.867	0.1	0.0628	1256.383	79.044
0.2	2.271	13.556	0.01	1355.661	0.05	0.0628	1352.986	85.122
0.4	2.495	14.893	0.01	1489.375	0.025	0.0628	1486.436	93.518
0.6	2.629	15.688	0.01	1568.897	0.015	0.0565	1566.389	88.671
0.8	2.696	16.090	0.01	1609.040	0.0125	0.0628	1605.856	101.032
1	2.756	16.448	0.01	1644.892	0.01	0.0628	1641.646	103.283
2	2.865	17.098	0.01	1709.893	0.005	0.0628	1706.518	107.364
4	2.920	17.425	0.01	1742.593	0.0025	0.0628	1739.154	109.418
6	2.917	17.406	0.01	1740.683	0.0015	0.0565	1737.901	98.380
8	2.927	17.466	0.01	1746.669	0.00125	0.0628	1743.223	109.674
10	2.913	17.385	0.01	1738.552	0.001	0.0628	1735.122	109.164

Table 8.4: Values obtained in the frequency sweep illustrated in figure 6.6 . The parameters used are listed in table 6.3 . The value of n_4 is set as 1.0 $\left(10^{23}\mathrm{m}^{-3}\right)$.

ω (Hz)	Torque (10^{-4}Nm)	Shear Stress (Pa)	Shear Strain	Shear Modullus (Pa)	Delay (s)	Delay (rad)	G' (Pa)	G" (Pa)
0.1	1.286	7.675	0.01	767.501	0.1	0.0628	765.987	48.191
0.2	1.416	8.449	0.01	844.904	0.05	0.0628	843.237	53.051
0.4	1.600	9.548	0.01	954.876	0.025	0.0628	952.992	59.957
0.6	1.704	10.172	0.01	1017.240	0.015	0.0565	1015.614	57.492
0.8	1.764	10.528	0.01	1052.882	0.0125	0.0628	1050.968	63.469
1	1.810	10.802	0.01	1080.247	0.01	0.0628	1078.116	67.829
2	1.885	11.251	0.01	1125.123	0.005	0.0628	1122.903	70.646
4	1.934	11.545	0.01	1154.535	0.0025	0.0628	1152.257	72.493
6	1.935	11.546	0.01	1154.636	0.0015	0.0565	1152.791	65.258
8	1.940	11.577	0.01	1157.722	0.00125	0.0628	1155.437	72.693
10	1.932	11.528	0.01	1152.876	0.001	0.0628	1150.601	72.389

Table 8.5: Values obtained in the frequency sweep illustrated in figure 6.6 . The parameters used are listed in table 6.3 . The value of n_4 is set as 0.8 $\left(10^{23}\mathrm{m}^{-3}\right)$.

ω (Hz)	Torque (10^{-4}Nm)	Shear Stress (Pa)	Shear Strain	Shear Modullus (Pa)	Delay (s)	Delay (rad)	G' (Pa)	G" (Pa)
0.1	1.253	7.478	0.01	747.806	0.1	0.0628	746.330	46.955
0.2	1.386	8.269	0.01	826.963	0.05	0.0628	825.332	51.925
0.4	1.568	9.356	0.01	935.623	0.025	0.0628	933.776	58.748
0.6	1.677	10.007	0.01	1000.761	0.015	0.0565	999.161	56.561
0.8	1.737	10.366	0.01	1036.601	0.0125	0.0628	1034.716	62.488
1	1.782	10.634	0.01	1063.452	0.01	0.0628	1061.354	66.774
2	1.866	11.134	0.01	1113.461	0.005	0.0628	1111.264	69.914
4	1.906	11.373	0.01	1137.382	0.0025	0.0628	1135.138	71.416
6	1.907	11.380	0.01	1138.015	0.0015	0.0565	1136.195	64.318
8	1.886	11.255	0.01	1125.535	0.00125	0.0628	1123.314	70.672
10	1.877	11.201	0.01	1120.104	0.001	0.0628	1117.893	70.331

Table 8.6: Values obtained in the frequency sweep illustrated in figure 6.6 . The parameters used are listed in table 6.3 . The value of n_4 is set as 0.01 $\left(10^{23}\mathrm{m}^{-3}\right)$.

ω (Hz)	Torque (10^{-5}Nm)	Shear Stress (Pa)	Shear Strain	Shear Modullus (Pa)	Delay (s)	Delay (rad)	G' (Pa)	G" (Pa)
0.1	7.254	4.329	0.01	432.962	0.3	0.188	425.293	81.129
0.2	8.913	5.319	0.01	531.977	0.15	0.188	522.554	99.682
0.4	1.123	6.701	0.01	670.134	0.075	0.188	658.264	125.570
0.6	1.245	7.433	0.01	743.311	0.04	0.150	734.876	111.664
0.8	1.319	7.869	0.01	786.988	0.02	0.100	783.014	78.983
1	1.365	8.148	0.01	814.860	0.015	0.094	811.243	76.685
2	1.467	8.754	0.01	875.462	0.005	0.0628	873.734	54.970
4	1.508	8.998	0.01	899.842	0.0025	0.0628	898.067	56.501
6	1.514	9.037	0.01	903.728	0.0015	0.0565	902.283	51.077
8	1.514	9.037	0.01	903.722	0.00125	0.0628	901.939	56.745
10	1.510	9.014	0.01	901.424	0.001	0.0628	899.645	56.600

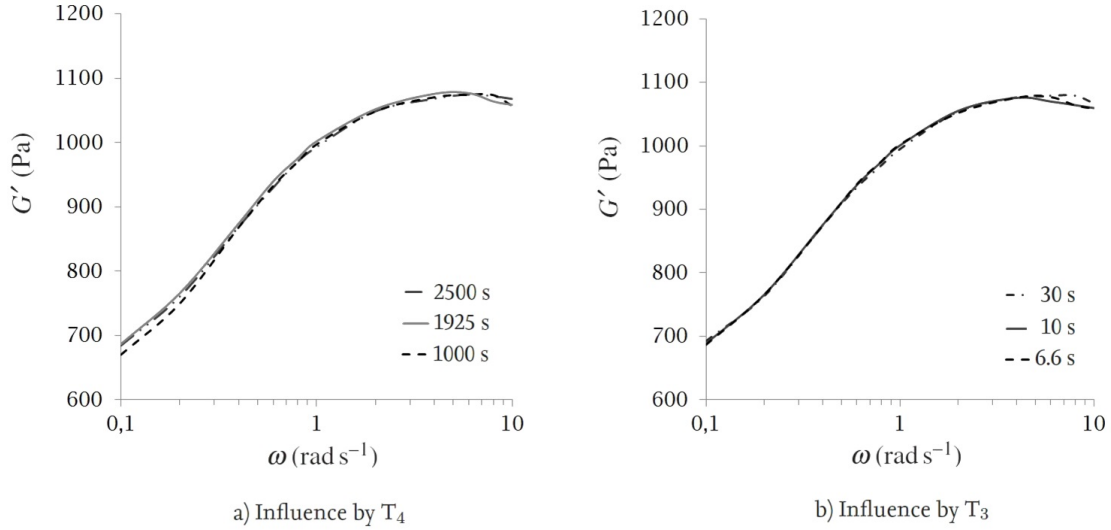

Figure 8.1: Frequency sweeps performed by studying the influence of relaxation times: a) Variation of T_4; b) Variation of T_3. The results suggest that for the chosen values of these relaxation times there is no influence in the range of 0.1 Hz to 10 Hz.

Table 8.7: Values obtained in the frequency sweep illustrated in figure 6.7 . The parameters used are listed in table 6.4 . The value of n_4 is set as 0.7 $\left(10^{23}\mathrm{m}^{-3}\right)$.

ω (Hz)	Torque (10^{-4}Nm)	Shear Stress (Pa)	Shear Strain	Shear Modullus (Pa)	Delay (s)	Delay (rad)	G' (Pa)	G" (Pa)
0.1	1.627	9.709	0.01	970.913	0.1	0.0628	968.997	60.964
0.2	1.683	10.047	0.01	1004.724	0.05	0.0628	1002.741	63.087
0.4	1.763	10.519	0.01	1051.981	0.025	0.0628	1049.905	66.054
0.6	1.776	10.599	0.01	1059.954	0.015	0.0565	1058.260	59.907
0.8	1.785	10.654	0.01	1065.481	0.012	0.0603	1063.543	64.229
1	1.797	10.724	0.01	1072.446	0.01	0.0628	1070.330	67.339
2	1.821	10.870	0.01	1087.063	0.005	0.0628	1084.917	68.257
4	1.826	10.900	0.01	1090.011	0.0025	0.0628	1087.860	68.442
6	1.827	10.904	0.01	1090.429	0.0015	0.0565	1088.686	61.629
8	1.832	10.931	0.01	1093.174	0.00125	0.0628	1091.017	68.640
10	1.830	10.930	0.01	1093.025	0.001	0.0628	1090.868	68.631

Table 8.8: Values obtained in the frequency sweep illustrated in figure 6.7 . The parameters used are listed in table 6.4 . The value of n_4 is set as 0.6 $\left(10^{23}\mathrm{m}^{-3}\right)$.

ω (Hz)	Torque (10^{-4}Nm)	Shear Stress (Pa)	Shear Strain	Shear Modullus (Pa)	Delay (s)	Delay (rad)	G' (Pa)	G" (Pa)
0.1	1.558	9.300	0.01	930.018	0.1	0.0628	928.183	58.396
0.2	1.608	9.597	0.01	959.752	0.05	0.0628	957.859	60.263
0.4	1.688	10.075	0.01	1007.583	0.025	0.0628	1005.595	63.266
0.6	1.712	10.218	0.01	1021.817	0.015	0.0565	1020.184	57.751
0.8	1.718	10.252	0.01	1025.295	0.012	0.0603	1023.430	61.806
1	1.723	10.282	0.01	1028.269	0.01	0.0628	1026.240	64.565
2	1.748	10.432	0.01	1043.232	0.005	0.0628	1041.173	65.505
4	1.752	10.458	0.01	1045.864	0.0025	0.0628	1043.800	65.670
6	1.754	10.465	0.01	1046.586	0.0015	0.0565	1044.913	59.151
8	1.760	10.498	0.01	1049.868	0.00125	0.0628	1047.797	65.921
10	1.760	10.498	0.01	1049.868	0.001	0.0628	1047.797	65.921

Table 8.9: Values obtained in the frequency sweep illustrated in figure 6.7 . The parameters used are listed in table 6.4 . The value of n_4 is set as 0.4 $\left(10^{23}\mathrm{m}^{-3}\right)$.

ω (Hz)	Torque (10^{-4}Nm)	Shear Stress (Pa)	Shear Strain	Shear Modullus (Pa)	Delay (s)	Delay (rad)	G' (Pa)	G" (Pa)
0.1	1.408	8.400	0.01	840.088	0.1	0.0628	838.430	52.749
0.2	1.457	8.698	0.01	869.810	0.05	0.0628	868.094	54.615
0.4	1.539	9.187	0.01	918.780	0.025	0.0628	916.967	57.690
0.6	1.564	9.335	0.01	933.599	0.015	0.0565	932.107	52.765
0.8	1.572	9.380	0.01	938.046	0.012	0.0603	936.340	56.547
1	1.585	9.458	0.01	945.888	0.01	0.0628	944.022	59.392
2	1.601	9.555	0.01	955.563	0.005	0.0628	953.677	60.000
4	1.604	9.575	0.01	957.574	0.0025	0.0628	955.684	60.126
6	1.607	9.588	0.01	958.899	0.0015	0.0565	957.366	54.195
8	1.610	9.628	0.01	962.814	0.00125	0.0628	960.914	60.455
10	1.610	9.635	0.01	963.560	0.001	0.0628	961.659	60.502

Table 8.10: Values obtained in the frequency sweep illustrated in figure 6.8 . The parameters used are listed in table 6.5 . The value of T_3 is set as 500 s.

ω (Hz)	Torque (10^{-4}Nm)	Shear Stress (Pa)	Shear Strain	Shear Modullus (Pa)	Delay (s)	Delay (rad)	G' (Pa)	G" (Pa)
0.1	1.379	8.228	0.01	822.875	0.1	0.0628	821.251	51.668
0.2	1.428	8.521	0.01	852.114	0.05	0.0628	850.432	53.504
0.4	1.495	8.925	0.01	892.507	0.025	0.0628	890.746	56.040
0.6	1.540	9.190	0.01	919.031	0.015	0.0565	917.562	51.942
0.8	1.549	9.246	0.01	924.635	0.012	0.0603	922.953	55.738
1	1.572	9.383	0.01	938.356	0.01	0.0628	936.504	58.919
2	1.596	9.522	0.01	952.250	0.005	0.0628	950.371	59.792
4	1.598	9.539	0.01	953.933	0.0025	0.0628	952.051	59.897
6	1.588	9.480	0.01	948.013	0.0015	0.0565	946.497	53.580
8	1.570	9.361	0.01	936.124	0.00125	0.0628	934.277	58.779
10	1.570	9.354	0.01	935.414	0.001	0.0628	933.568	58.734

Table 8.11: Values obtained in the frequency sweep illustrated in figure 6.8 . The parameters used are listed in table 6.5 . The value of T_3 is set as 1000 s.

ω (Hz)	Torque (10^{-4}Nm)	Shear Stress (Pa)	Shear Strain	Shear Modullus (Pa)	Delay (s)	Delay (rad)	G' (Pa)	G" (Pa)
0.1	1.385	8.268	0.01	826.826	0.1	0.0628	825.195	51.916
0.2	1.437	8.573	0.01	857.360	0.05	0.0628	855.668	53.834
0.4	1.516	9.050	0.01	905.023	0.025	0.0628	903.237	56.826
0.6	1.556	9.287	0.01	928.711	0.015	0.0565	927.227	52.489
0.8	1.571	9.374	0.01	937.449	0.012	0.0603	935.744	56.511
1	1.585	9.461	0.01	946.169	0.01	0.0628	944.301	59.410
2	1.600	9.550	0.01	955.055	0.005	0.0628	953.171	59.968
4	1.602	9.560	0.01	956.094	0.0025	0.0628	954.207	60.033
6	1.591	9.494	0.01	949.403	0.0015	0.0565	947.886	53.658
8	1.580	9.409	0.01	940.904	0.00125	0.0628	939.048	59.079
10	1.570	9.384	0.01	938.451	0.001	0.0628	939.600	58.925

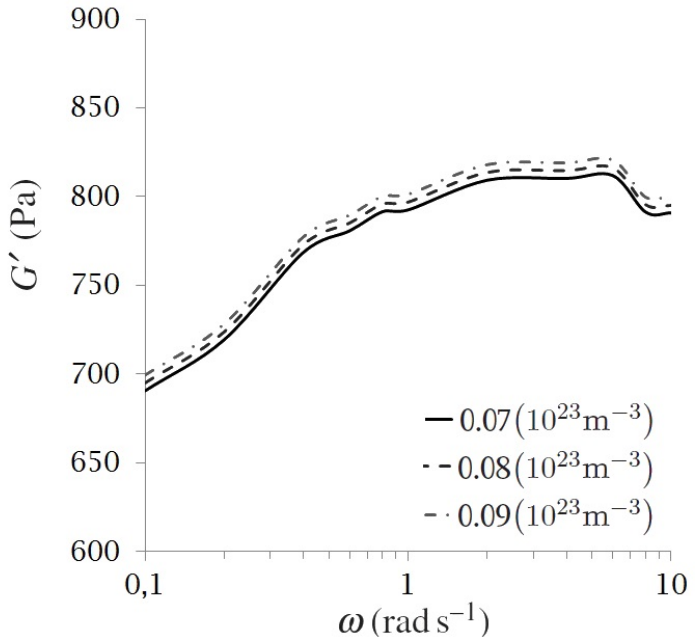

Figure 8.2: Influence of the number of chains per network n_4 by taking the relaxation time T_3 as 100s. The results suggest that for the chosen values of these number of chains there is only little difference between the curves obtained in the range of 0.1 Hz to 10 Hz. Decreasing the number of chains n_4 it is decreased again only the material stiffness.

Table 8.12: Values obtained in the frequency sweep using the parameters listed in table 6.6. It is simulated the rheological model of Gellan with calcium cations.

ω (Hz)	Torque (10^{-4}Nm)	Shear Stress (Pa)	Shear Strain	Shear Modullus (Pa)	Delay (s)	Delay (rad)	G' (Pa)	G" (Pa)
0.1	1.418	8.464	0.01	846.480	0.1	0.0628	844.809	53.150
0.2	1.479	8.828	0.01	882.869	0.05	0.0628	881.126	55.435
0.4	1.561	9.317	0.01	931.755	0.025	0.0628	929.916	58.505
0.6	1.593	9.507	0.01	950.764	0.015	0.0565	949.244	53.735
0.8	1.608	9.594	0.01	959.418	0.012	0.0603	957.673	57.835
1	1.622	9.682	0.01	968.257	0.01	0.0628	966.347	60.797
2	1.637	9.769	0.01	976.971	0.005	0.0628	975.043	61.344
4	1.639	9.781	0.01	978.171	0.0025	0.0628	976.240	61.419
6	1.627	9.713	0.01	971.325	0.002	0.0753	968.565	73.166
8	1.640	9.774	0.01	977.490	0.0017	0.0879	973.711	85.873
10	1.630	9.750	0.01	975.001	0.0015	0.0942	970.674	91.755

Table 8.13: Values obtained in the frequency sweep using the parameters listed in table 6.7. It is simulated the rheological model of Gellan with magnesium cations.

ω (Hz)	Torque (10^{-4}Nm)	Shear Stress (Pa)	Shear Strain	Shear Modullus (Pa)	Delay (s)	Delay (rad)	G' (Pa)	G" (Pa)
0.1	1.160	6.920	0.01	692.032	0.1	0.0628	690.666	43.453
0.2	1.208	7.208	0.01	720.894	0.05	0.0628	719.472	45.265
0.4	1.290	7.701	0.01	770.175	0.025	0.0628	768.655	48.359
0.6	1.310	7.820	0.01	782.082	0.015	0.0565	780.832	44.202
0.8	1.329	7.930	0.01	793.057	0.012	0.0603	791.615	47.807
1	1.331	7.941	0.01	794.138	0.01	0.0628	792.571	49.864
2	1.359	8.109	0.01	810.915	0.005	0.0628	809.314	50.917
4	1.360	8.118	0.01	811.893	0.0025	0.0628	810.291	50.979
6	1.364	8.142	0.01	814.221	0.002	0.0753	811.908	61.332
8	1.330	7.944	0.01	794.412	0.0017	0.0879	791.341	69.790
10	1.330	7.944	0.01	794.412	0.0015	0.0942	790.887	74.760

Bibliography

[1] D. Monroe. Looking for chinks in the armor of bacterial biofilms. *PLoS Biol.*, 5:11, 2007.

[2] R. Moreno. Reología de suspensiones cerámicas. *Bol. Soc. Esp. Ceram. Vidr.*, 39:601–608, 2000.

[3] G. Schramm. *A practical approach to Rheology and Rheometry*. Thermo Electron Company GmbH, 2004.

[4] J.T. Celigüeta. Introducción al análisis de estructuras con no linealidad geométrica. Technical report, Tecnun, 2008.

[5] A.E. Ehret and M. Böl. Modelling mechanical characteristics of microbial biofilms by network theory. *J. R. Soc. Interface.*, 6:13, 2012.

[6] Instruments Bohlin. *Benutzerhandbuch für Bohlin Rheometer*. Bohlin Instruments Gmbh, 2001.

[7] M. Wloka, H. Rehage, H.C. Flemming, and J. Wingender. Structure and rheological behavior of the extracellular polymeric substance network of mucoid pseudomonas aeruginosa biofilms. *Biofilms*, 2:275–283, 2005.

[8] P. Stoodley, R. Cargo, C.J. Rupp, S. Wilson, and I. Klapper. Biofilm material properties as related to shear-induced deformation and detachment phenomena. *Ind. Microbiol. Biotech.*, 29:361–367, 2002.

[9] H.C. Flemming, J. Wingender, C. Mayer, V. Korstgens, and W. Borchard. Cohesiveness in biofilm matrix polymers. Technical report, Cambridge University Press, Cambridge., 2000.

[10] C. Mayer, R. Moritz, C. Mayer, R. Moritz, C. Kirschner, W. Borchard, R. Maibaum, J. Wingender, and H. C. Flemming. The role of intermolecular interactions: studies on model systems for bacterial biofilms. *Int J Biol Macromol*, 26:3–16, 1999.

[11] D. Kaptsan. Rheologishe charakterisierung und etablierung von viskoelastischen hydrogelen als modellbiofilm. Master's thesis, Institut fur Bioverfahrenstechnik, 2012.

[12] J.W. Costeron. Overview of microbial biofilms. *Indus. Microbiol.*, 15:137–140, 1995.

[13] J.C. Post, P. Stoodley, l. Hall-Stoodley, and G.D. Ehrlich. The role of biofilms in otolaryngologic infections. *Curr Opin Otolaryngol Head Neck Surg 2004*, 12:185–90, 2004.

[14] J.W. Costerton, P.S. Stewart, and E.P. Greenberg. Bacterial biofilms: a common cause of persistent infections. *Science*, 284:1318–1322, 1999.

[15] S. Fuchs, T. Haritopoulou, and M. Wilhelmi. Biofilms in freshwater ecosystems and their use as pollutant monitor. *Water Sci. Technol.*, 37:137–40, 1996.

[16] A. Dermici and I. Pometto. Repeated batch fermentation in biofilm reactors with plastic- composite supports for lactic acid production. *Appl. Environ.Microbiol.*, 43:585–590, 1995.

[17] S. Marques and J.L. Ramos. Transcriptional control of the pseudomonas putida tol plasmid catabolic pathways. *Molecular Microbiology*, 9:923–929, 1993.

[18] E.R. Olivera, D. Carnicero, R. Jodra, B. Miñambres, B. García, and G.A. Abraham. Genetically engineered pseudomonas: a factory of new bioplastics with broad applications. *Environmental Microbiology*, 3:612, 2001.

[19] M. Böl, A. E. Ehret, A. Bolea Albero, J. Hellriegel, and R. Krull. Recent advances in mechanical characterisation of biofilm and their significance for material modelling. *Critical Reviews in Biotechnology*, 1:1–27, 2012.

[20] W.G. Characklis. Biofilm development and destruction. Technical report, Electric Power Research Institute, Palo Alto, CA., 1980.

[21] B.E. Christensen and W.G. Characklis. Physical and chemical properties of biofilms. *Biofilms. John Wiley&Sons, Inc*, 5:93–130, 1990.

[22] A. Ohashi and H. Harada. A novel concept for evaluation of biofilm adhesion strength by applying tensile force and shear force. *Water Science and Technology*, 34:201–211, 1996.

[23] A. Ohashi, T. Koyama, K. Syutsubo, and H. Harada. A novel method for evaluation of biofilm tensile strength resisting erosion. *Water Science and Technology*, 39:261–268, 1999.

[24] P. Stoodley, Z. Lewandowski, J.D. Boyle, and H.M. Lappin-Scott. Structural deformation of bacterial biofilms caused by short-term fluctuations in fluid shear: An in situ investigation of biofilm rheology. *Biotech. Bioeng*, 65:83–92, 1999.

[25] I. Klapper, C.J. Rupp, R. Cargo, B. Purvedorj, and P. Stoodley. Viscoelastic fluid description of bacterial biofilm material properties. *Biotechnol. Bioeng*, 80:289–296, 2002.

[26] B.W. Towler, C.J. Rupp, A.B. Cunningham, and P. Stoodley. Viscoelastic properties of a mixed culture biofilm from rheometer creep analysis. *Biofouling*, 19:279–285, 2003.

[27] V. Korstgens, H.C. Flemming, J. Wingender, and W. Borchard. Uniaxial compression measurement device for investigation of the mechanical stability of biofilms. *Microbiol. Meth.*, 46:9–17, 2001.

[28] M.J. Chen, Z. Zhang, and T.R. Bott. Effects of operating conditions onthe adhesive strength of pseudomonas fluorescens biofilms in tubes. *Colloid. Surface*, 43:61–71, 2005.

[29] E.H. Poppele and R.M. Hozalski. Micro-cantilever method formeasuring the tensile strength of biofilms and microbial flocs. *Microbiol. Meth.*, 55:607–615, 2003.

[30] F. Ahimou, M.J. Semmens, P.J. Novak, and Haugstad G. Biofilm cohesiveness measurement using a novel atomic force microscopy methodology. *Appl. Environ. Microbiol*, 73:2897–2904, 2007.

[31] R.B. Mohle, T. Langemann, M. Haesner, W. Augustin, S. Scholl, T.R. Neu, D.C. Hempel, and H. Horn. Structure and shear strength of microbial biofilms as determined with confocal laser scanning microscopy and fluid dynamic gauging using a novel rotating disc biofilm reactor. *Biotechnol. Bioeng.*, 98:747–755, 2007.

[32] C. Picioreanu, M.C.M. Loosdrecht, and J.J. Heijnen. Twodimensionalmodel of biofilm detachment caused by internal stress from liquid flow. *Biotechnol. Bioeng.*, 72:205–218, 2001.

[33] V. Korstgens, H.C. Flemming, J. Wingender, and W. Borchard. Influence of calcium ions on the mechanical properties of a model biofilm of mucoid pseudomonas aeruginosa. *Wat. Sci. Technol.*, 43:49–57, 2001.

[34] D.G. Davies, M.R. Parsek, J.P. Pearson, B.H. Iglewski, J.W. Costerton, and E.P. Greenberg. The involvement of cell-to-cell signals in the development of a bacterial biofilm. *Science*, 280:295–298, 1998.

[35] J.D. Ferry. *Viscoelastic Properties of Polymers*. J. Wiley and Sons, 1980.

[36] O. Lieleg, M. Caldara, R. Baumgärtel, and K. Ribbeck. Mechanical robustness of pseudomonas aeruginosa biofilms. *Soft Matter*, 7:3307–3314, 2011.

[37] R.W. Ogden. Non-linear elastic deformations. Technical report, Dover Publications, 1997.

[38] S.M. Green and A.V. Tobolsky. A new approach to the theory of relaxing polymeric media. *J. Chem. Phys.*, 14:80–92, 1946.

[39] B. Bernstein, E.A. Kearsley, and L.J. Zapas. A study of stress relaxation with finite strain. *Trans. Soc. Rheol.*, 7:391–410, 1963.

[40] H.A. Barnes. *A Handbook of Elementary Rheology*. Institute of Non-Newtonian Fluid Mechanics University of Wales, 2000.

[41] M. Wloka, H. Rehage, H.C. Flemming, and J. Wingender. Rheological properties of viscoelastic biofilm extracellular polymeric substances and comparison to the behavior of calcium alginate gels. *Colloid Polym. Sci.*, 282:1067–1076, 2004.

[42] V.A. Hackley and C.F. Ferraris. Guide to rheological nomenclature: Measurements in ceramic particulate systems. Technical report, NIST Special Publication, 2001.

[43] ABAQUS. *ABAQUS/CAE User's Manual*, abaqus version 6.5 edition, 2004.

[44] I.M.N. Vold, K.A. Kristiansen, and B.E. Christensen. A study of the chain stiffness and extension of alginates, in vitro epimerized alginates, and periodate-oxidized alginates using size-exclusion chromatography combined with light scattering and viscosity detectors. *Biomacromolecules*, 7:2136–2146, 2006.

[45] J.T. Oliveira, L. Martins, R. Piccionchi, P.B. Malafaya, and R.A. Sousa. Gellan gum: A new biomaterial for cartilage tissue engineering applications. *Biomedical Materials Research*, 1:852–63, 2010.

[46] P.B. Deasy and K.J. Quigley. Rheological evaluation of deacetylated gellan gum (gelrite) for pharmaceutical use. *International Journal of Pharmaceutics*, 73:117–123, 1991.

[47] K.S. Hossain and K. Nishinari. Chain release behavior of gellan gels. *Colloid & Polymer Science*, 136:177–186, 2009.

[48] E. Miyoshi, T. Takaya, and K. Nishinari. Rheological and thermal studies of gel-sol transition in gellan gum aqueous solutions. *Carbohydrate Polymers*, 30:109–119, 1996.

[49] R. Takahashi, H. Tokunou, K. Kubota, E. Ogawa, T. Kawase, and K. Nishinari. Solution properties of gellan gum: Change in chain stiffness between single- and double-stranded chains. *Biomacromolecules*, 5:516–523, 2004.

[50] R. Takahashi, M. Akutu, K. Kubota, and K. Nakamura. Characterization of gellan gum in aqueous nacl solution. *Progress in Colloid and Polymer Science Volume*, 114:1–7, 1999.

Xabier Ocáriz Aguirre
Institut für Festkörpermechanik
Technische Universität Braunschweig
Schleinitzstraße 20
Postfach 3329
38106 Braunschweig